Submitted to the Astrophysical Journal

Simulating the Early Evolution of the Hard X-Ray Properties of a Young Stellar Population

Michael S. Sipior[1], Michael Eracleous, & Steinn Sigurdsson

Department of Astronomy and Astrophysics, The Pennsylvania State University, 525 Davey Lab, University Park, PA 16802

sipior@science.uva.nl, mce@astro.psu.edu, steinn@astro.psu.edu

ABSTRACT

We present an X-ray binary population synthesis model, and use it to simulate the evolution of X-ray binaries formed in a burst of star formation of duration 20 Myr and star-formation rate 10 $M_\odot$ yr^{-1}. Our goal is to explain the hard (2–10 keV) X-ray properties of populations of extragalactic X-ray binaries recently observed by the *Chandra* X-Ray Observatory, especially those associated with recent or ongoing episodes of vigorous star formation. Our simulated X-ray binary population reaches a maximum 2–10 keV luminosity of $\sim 4 \times 10^{40}$ erg s^{-1} after approximately 20 Myr. The X-ray luminous phase is sustained for a period of several hundreds of Myr by succeeding populations of systems with lighter secondary stars, i. e., it persists long after the star-formation episode has ended. These results are insensitive to the poorly-constrained values of the initial mass function and the average mass ratio between accreting and donor stars. The computed peak X-ray luminosity is consistent with observationally-derived correlations between the star-formation rate and the observed hard X-ray luminosity. Model cumulative luminosity functions at the earliest times have power-law indices in agreement with those derived from observations of actively star-forming galaxies. The model cumulative luminosity functions become increasingly steeper with time as the most luminous systems die off, which offers an explanation for the difference in the slopes of observed cumulative luminosity functions of young and old stellar populations.

Subject headings: stars: evolution – stars: formation – galaxies: starburst – X-rays: binaries – X-rays: galaxies

---

[1]Current address: Astronomical Institute "Anton Pannekoek" and Section Computational Science, University of Amsterdam, Kruislaan 403, 1098 SJ Amsterdam, Netherlands.

1. Introduction

1.1. X-Ray Binaries Revealed By *Chandra*

There is now a considerable corpus of evidence that, for "normal" galaxies (i. e. with no active nucleus), the principal component of the X-ray luminosity above 2 keV arises from the associated population of X-ray binaries (XRBs). This is especially true in the presence of vigorous starburst activity, and has been further established with the advent of the *Chandra* X-ray Observatory, where high-resolution imaging allows an accurate source census and luminosity function to be constructed for a diverse sample of host galaxies. Specific examples of large, luminous XRB populations that have been revealed with *Chandra* include the vigorous starbursts in NGC 4038/4039 (the Antennae, Fabbiano et al. 2001), M82 (Zezas et al. 2002; Griffiths et al. 2000), and the ULIRG NGC 3256 (Lira et al. 2002). Perhaps more interesting, however, has been the discovery of sizable XRB populations in non-starbursting galaxies, with inactive or mildly-active galactic nuclei, comparable to those found in some starbursts. The implication, given the generally slow star-formation rate (SFR), is that a significant fraction of X-ray binaries can remain luminous for many gigayears affecting the X-ray emission of a galaxy long after their formation. By way of example, NGC 1291 (Irwin et al. 2002), IC 5332, M83 (Kilgard et al. 2002), and NGC 4736 (Eracleous et al. 2002) all sport several dozen point sources with 2–10 keV X-ray luminosities well in excess of 10^{37} erg s^{-1}. The first two of these are undistinguished spirals; NGC 1291 has a current SFR several times lower than that seen in the Milky Way, at around 0.1 $M_\odot$ yr^{-1}(Caldwell et al. 1991), and yet the two galaxies have roughly comparable populations of luminous XRBs (Grimm et al. 2003), implying that their historical SFRs were similar. M83 is known to exhibit highly localized starburst activity in the nucleus and bar regions (Telesco et al. 1993), though the observed XRB population is not limited to these areas. The nucleus of NGC 4736 is known to contain a LINER (Low-Ionization Nuclear Emission Region; see Heckman 1980). Although some LINERs are powered by accretion onto a nuclear, supermassive black hole occupying the low end of the spectrum of nuclear activity, a significant fraction of them (perhaps the majority) are weak, compact starbursts. Such LINERs thus occupy the low end of the spectrum of starburst activity.

More than any other quantity observable in the X-ray band, the luminosity distribution of an XRB population gives great insight into the recent star formation history of the host galaxy. Measurements of soft X-ray superwinds provide a great deal of information on *recent* episodes of star formation; however, XRBs are more durable records of the recent past, and can be studied long after the star formation driving the superwind has faded. This may be particularly useful in galaxies with moderate SFRs (such as some LINERs), where a measurable superwind may simply never form.

With the above observational considerations in mind, we embarked on a theoretical study of the integrated hard X-ray properties of a young stellar population. Our primary goal was to simulate the formation and evolution of interacting binaries and to compute the evolution of the integrated X-ray luminosity as well as the statistical properties of the X-ray source population. The results of our study are the subject of this paper.

1.2. The Goals of Our Simulations

The immediate goal of the simulations undertaken here is to predict the evolution of the integrated hard X-ray luminosity of a young stellar population, formed in a recent episode of star formation, as well as the evolution of the luminosity function of its discrete X-ray sources. Therefore, we concentrate on the relatively simple problem of simulating a brief episode of steady star formation. Later work may focus on particular case studies in which individual galaxies are modeled using observational information on their SFRs and star-formation histories.

The evolution of the discrete-source luminosity function is of particular interest since recent observations show that it is closely related to recent or current star-formation activity. The analyses of Eracleous et al. (2002) and Kilgard et al. (2002) have shown that the luminosity function in starburst galaxies tends to be substantially flatter, with high-luminosity sources in greater abundance. Moreover, the slope of the luminosity function shows a strong correlation to the observed 60 μm and Hα luminosities, direct measures of star formation (Kennicutt 1983; Lonsdale Persson & Helou 1987; Devereux & Young 1990). This trend can be qualitatively understood in terms of the evolutionary time scales of various components of the XRB population. For low-mass X-ray binaries (LMXBs), mass transfer is driven by either the nuclear evolution of the donor or the loss of angular momentum through gravitational radiation and magnetic braking processes. All of these mechanisms operate over relatively long time scales. In contrast, high-mass X-ray binaries (HMXBs) begin mass transfer on the shorter nuclear time scale of the massive donor star. HMXBs powered by Roche-lobe overflow tend to be brighter, on average, than LMXBs, as the accretor is more likely to be a black hole when the donor is massive. The result is a flat luminosity function (more numerous bright X-ray sources) for young stellar populations, which slowly becomes steeper as the short-lived HMXBs give way to long-lived LMXBs. The quantitative investigation of the above processes is an important goal of the work presented here.

The problem of the long-term evolution of XRBs and its observational signatures has recently been approached in a semi-numerical fashion by Ghosh & White (2001); Ptak et al. (2001); White & Ghosh (1998), in addition to a completely analytic formalism presented in Wu (2001). Our goal is to approach the study of the evolution of galactic X-ray properties from a numerical standpoint, which requires fewer simplifying assumptions than a semi-numerical or purely analytic formulation.

2. Population Modeling

2.1. History and Authorship of the Population Synthesis Code

We make use of a binary evolution code detailed in part by Pols & Marinus (1994), and modified for use in neutron star-neutron star (NS-NS) systems by Bloom et al. (1999). Our extension of the code allows for evolution to the black hole state, with assumptions about the mass function of such objects at the time of collapse; in addition, the technique for computing mass transfer rates was refined considerably, by coupling it more directly to the underlying physics, as discussed below.

For purposes of the numerical model, an initial binary system is considered to be completely described by four parameters: the mass of the system's primary (more massive) star, M_1, which

is chosen from the specified initial mass function; the initial primary to secondary mass ratio, q, defined to lie between zero and unity; the initial orbital eccentricity, e; and the initial orbital semi-major axis, a. The code then evolves the binary in time, taking into account the orbital changes caused by mass transfer, wind loss, etc. These four quantities are tracked, as is the evolutionary state of each star, and any mass exchanges that take place. The simulation of the evolution of the binary ends when both stars have reached their respective evolutionary end points, which are a strict function of the initial core mass.

2.2. Population Code Theory of Operation, Choice and Extent of Parameter Space

The evolution of a binary pair starts with the choice of a primary mass from an assumed initial mass function (IMF). For this work, we consider two power law IMFs (where $dN = m^{-\alpha}dm$); the first index is $\alpha = -2.35$ (the Salpeter IMF; Salpeter 1955), the second is $\alpha = -2.7$, approximating the high end of a Miller-Scalo IMF (Miller & Scalo 1979). In both cases, we established a lower cutoff of 4 $M_\odot$ for the primary star's mass, confining the code to an interesting range of initial masses; i. e., where at least one supernova is possible in principle. This is because our interest is in systems with a neutron star or black hole, as these are the potentially luminous X-ray sources. Our stellar models are taken primarily from Maeder & Meynet (1989). The helium star models used are a mix of models from Habets (1986) and Paczynski (1971), and the reader is referred to these for a detailed discussion and evolutionary tracks.

The distribution of q is a topic of some controversy, given the observational biases involved in studying systems with diverse mass ratios (Hogeveen 1992). A "flat" distribution, where all values of q are equally likely, is often chosen given the difficulty in reconstructing the underlying function. An extensive inventory of observational data was compiled by Kuiper (1935) in an attempt to address the mass ratio distribution question. These data, coupled with the more recent data of Batten et al. (1989), and the analysis found in Hogeveen (1992), point to two principal results. First, in the case of single-lined spectroscopic binaries, the distribution of q is a two-part function, where:

$$\psi(q) \propto \begin{cases} q^{-2} & \text{for} \quad q > 0.3 \\ 1 & \text{for} \quad q < 0.3 \end{cases} \tag{1}$$

For double-lined spectroscopic systems, the observed q distribution was found to be driven almost completely by selection effects, albeit consistent with the q-distribution of single-lined binaries above. See Elson et al. (1998) for a further discussion of this problem in the context of massive binaries in a young LMC cluster, where a q distribution biased towards companions of equal mass is found, but the detection limit prevents an accurate census of low-q systems. We consider both the flat and the low-skewed q-distributions in our simulations below, accepting that reality likely lies somewhere between these two points.

The initial binary separation is chosen after Abt (1983), with a distribution that is flat in the logarithm of the semi-major axis , and in the range $10\,R_\odot < a < 10^6\,R_\odot$. This distribution fits well with existing spectroscopic surveys of nearby stars. Duquennoy & Mayor (1991), describe another separation distribution, based upon a CORAVEL spectroscopic survey of 181 Gliese catalogue stars. The function they derive is Gaussian, with a mean of 8×10^3 $R_\odot$ and a dispersion of 8×10^2 $R_\odot$.

We use Abt's prescription here, but wished to make clear that this is not a settled issue. Related population synthesis studies currently use the former distribution almost exclusively, often with little comment. If the Duquennoy & Mayor (1991) result holds when expanded to a larger survey size (preferably including a few non-local systems) then this issue will have to be revisited. Given the dramatically wider initial separations implied by the Duquennoy & Mayor (1991) distribution, one can at least make the prediction that far fewer X-ray binaries would result, since the common-envelope phase would be less likely to occur. This in turn would imply wider systems with larger Roche surfaces, making Roche-lobe overflow less likely.

The eccentricity is chosen from the standard thermal distribution, $\xi(e) = 2e$. This choice for the distribution of initial eccentricities is ubiquitous in binary population synthesis. The mathematics justifying this relation can be found in Heggie (1975), and interested readers are referred there for all of the details.

After the initial parameters have been selected, each binary system is evolved along the stellar tracks referenced above until both components have reached their final degenerate form, accounting for mass-transfer-induced stellar regeneration and stellar winds. Stellar winds from helium stars are accounted for using the relation developed in Langer (1989), where the mass loss rate is $\dot{M} = 5 \times 10^{-8}\ (M/\mathrm{M}_{\odot})^{2.5}\ \mathrm{M}_{\odot}\ \mathrm{yr}^{-1}$. This wind lasts for the duration of the star's helium main sequence lifetime.

When the more massive primary leaves the main sequence and ascends the giant branch, the rapidly-swelling star may engulf its companion with its outer envelope. This common-envelope phase will rapidly shrink the orbital radius of the binary on a time scale of only a few orbital periods. Those systems that avoid a merger event at the end of the common-envelope phase will be more likely to engage in mass transfer, as the size of the companion's Roche lobe shrinks along with the orbital separation. A common-envelope phase can also result as the secondary leaves the main sequence, though systems are unlikely to survive two such events without merging. For our purposes here, during the common-envelope phase, the orbit is circularized, and the orbital energy is reduced by the binding energy of the envelope divided by the common-envelope efficiency parameter, which we take to be 0.5. In other words, the orbital energy is reduced by twice the envelope binding energy. The common-envelope efficiency is just the fraction of the binary orbital energy which is required to eject the common envelope. The value of this quantity is contentious at present, as the microphysics necessary to model such an environment is poorly understood. Attempts at estimating this parameter can be found in Livio & Soker (1988), Rasio & Livio (1996) and Dewi & Tauris (2000), among others.

Neutron stars are formed from progenitors with zero-age main sequence (ZAMS) masses of between 8 and 20 $\mathrm{M}_{\odot}$, inclusive, and are always given a mass of 1.4 $\mathrm{M}_{\odot}$. More massive stars end up as black holes. This boundary is unlikely to be a sharp one, as it is strongly coupled to the spin state of the pre-collapse object (Fryer 1999). Even assuming this was known to perfect accuracy, the effects of magnetic fields and rotational support on the compact object's end state are not well understood. This point also bears upon the magnitude and direction distribution of natal kicks received by the neutron star at birth, from an asymmetric emission of neutrinos or core material. The role of and justification for asymmetric natal kicks is discussed below, including the appearance of asymmetric kicks during black hole formation.

The black hole mass function (i. e., the post-collapse mass of a black hole, given its mass just prior to the explosion) is highly speculative at this point, and is almost certainly not merely a function of initial mass, but also of angular momentum, to the extent that this determines the fraction of material falling back onto the collapsing star. In order to experience a kick, the black hole's formation must be delayed somewhat, either due to rotational support, or because event horizon formation occurs only after delayed fallback of mass initially ejected from the core. Fryer (1999) has performed core-collapse simulations in order to explore the critical mass for black hole formation, and the final masses of the resulting black holes. As a best working scenario, we have constructed a mass relation from a quadratic fit to the limited data set found in Fryer (1999). Our fit shows that the mass of the black hole at formation (M_{BH}) is related to the ZAMS mass of the progenitor (M_0) by $M_{BH} = (M_0/25\ \mathrm{M}_\odot)^2 \times 5.2\ \mathrm{M}_\odot$. This relation is accurate to about 10% of the black hole initial mass at each of the values resulting from a hydrodynamic simulation. It should be noted that this relation is almost certainly dependent upon metallicity (see, for example, Fryer et al. 2002). The assumed relation is appropriate for systems with approximately solar metallicity, but would need to be adjusted to represent metal-poor progenitors.

The importance of the black hole IMF in XRB formation extends beyond the obvious effect on a system's orbital elements. The maximum luminosity from future mass transfer onto the black hole is a function of the hole mass. The Eddington limit, $L_{Edd} = 1.3 \times 10^{38}\ (M/\mathrm{M}_\odot)$ erg s^{-1}, is frequently invoked for this luminosity cutoff; however, this limit applies strictly only in the case of spherically symmetric accretion. The black hole IMF is important because it is one of two important factors that set the maximum luminosity of the most luminous XRBs (the other is the range of mass transfer rates from the companion star). Thus, the high-luminosity end of the resulting luminosity function depends quite sensitively on the black hole IMF.

Of course, the Eddington assumption can be relaxed, allowing us to test the models that have been put forward to explain the significant number of extremely-luminous XRBs now known to exist. Models that explain these events through *bona fide* super-Eddington accretion (Begelman 2002) should result in a different luminosity distribution and number of sources (per unit SFR) than models involving randomly-directed relativistic beaming (King et al. 2001). Careful population synthesis can provide a means to discriminate between these hypotheses, and we hope to report the result in the near future.

Another relevant parameter concerns the magnitude of natal kicks to be imparted to a neutron star or black hole at formation. There are two mechanisms for natal kicks. First, Blaauw-Boersma kicks (Blaauw 1961) resulting from conservation of momentum after the supernova which gives birth to the compact object. Second, asymmetric kicks arise from the anisotropic emission of neutrinos and/or core material in the supernova event. Compared to symmetric Blaauw-Boersma kicks, a smaller amount of mass loss is needed to generate a comparable velocity change, and this is especially true if the bulk of the momentum is carried away in an anisotropic neutrino flux. For neutron stars formed in a supernova, this scenario is sufficient. However, if the star is massive enough to form a black hole, there is a potential problem for the natal kick scenario. Gourgoulhon & Haensel (1993) convincingly demonstrate that, if the event horizon forms on the dynamical time scale of the collapsing core, an insufficient number of neutrinos escape to drive a supernova explosion through envelope heating. This implies a maximum mass for a supernova progenitor, above which the supernova is quenched by the event horizon before it begins. We have chosen a simple criterion

for whether a black hole will receive an asymmetric kick during collapse; namely, all objects below 40 $M_\odot$ (referring to the ZAMS mass) experience a random kick. Above this limit, objects collapse directly to a black hole, with no kick. This is a simplification consistent with hydrodynamical simulations such as those of Janka & Mueller (1996), Fryer (1999) and Fryer & Heger (2000).

The magnitude and direction of the asymmetric kick are still matters of considerable debate. One strong possibility is that of neutrino-induced convection, as discussed in Janka & Mueller (1994); Fryer & Heger (2000), and references therein. In this process, the angular momentum acts to stabilize the forming compact object, so that rapidly-rotating progenitors produce substantially-weakened explosions. The neutrino convection in rapid-rotators is concentrated at the slowly-rotating poles, driving an asymmetrical supernova. It is interesting that the kick vector depends not only upon the rotation of the progenitor, but that an inverse correlation is posited between the magnitude of the supernova event and the asymmetry of the explosion. Unfortunately, the binary evolution code does not track the rotation state of the progenitor, and so while the above theoretical predictions are an interesting path for future investigations, they cannot be effectively applied here. Therefore, we take asymmetric kicks to be oriented isotropically. The imparted kick speed is selected from a Maxwellian distribution with an energy corresponding to a 1.4 $M_\odot$neutron star with a speed of 90 km s^{-1}. The distribution is truncated at the high end, with a maximum kick speed of 500 km s^{-1} (again, for a 1.4 $M_\odot$neutron star). All kick speeds are scaled to the mass of the recoiling object; e. g., a 7 $M_\odot$black hole will receive a speed change one-fifth the size that would be imparted to the aforementioned neutron star. This kick is slightly lower than that posited by Hansen & Phinney (1997), and we do not consider the possibility of a bifurcated kick distribution put forward in recent literature (Arzoumanian et al. 2002; Pfahl et al. 2002).

It is important to note that, in order for a system to become an XRB of any type, it must first survive the natal kick produced when the compact object is formed. The likelihood of this obviously drops dramatically as the imparted kick speed increases. Since the kick speed is inversely proportional to the mass of the compact object progenitor, an immediate prediction is that XRBs with a black hole accretor should be more common than the assumed IMF would indicate, as these systems will survive the first natal kick more easily than systems with a neutron star primary. A similar effect holds for the mass of the donor star, though in this case the effect is independent of the kick magnitude. Systems which retain a larger fraction of their total mass have a greater chance of surviving the first supernova; this implies that binaries with more massive secondaries are also more resistant to disruption. The overall effect is to increase the ratio of HMXB to LMXB systems compared to what would be predicted on the basis of the initial IMF alone.

2.3. Implementation of Mass Transfer in the Code

The code itself tracks changes of state, which means that instead of evolving a binary system along a smoothly-flowing time axis, the next evolutionary "event" (for example, a star may leave the main sequence, or become a helium star after casting off its envelope through a stellar wind) is found from the input stellar evolution tracks, and the code advances the time index accordingly. At this point the code extrapolates mass loss from winds for each star for the elapsed time, and recalculates orbital parameters accordingly. Sudden mass loss (from supernova events) is handled

identically, with the code reporting the evolutionary state and orbital parameters immediately before the explosion, and immediately after. If, after advancing to the next evolutionary state, the code determines that the two stars should have interacted via mass transfer at some point, the system is backed up to the immediately previous state, and the orbital parameters are set such that (at least) one star is barely in contact with its Roche-lobe. An episode of mass transfer is then resolved, ending with both stars inside their respective Roche-lobes (or with a spiral-in, if the system was undergoing common-envelope evolution and lost sufficient orbital energy to bring the stellar cores into contact, after ejecting the envelope).

Mass transfer rates were computed following the model of Hurley et al. (2002), and references therein. To determine the stability and time scale of mass transfer, adiabatic coefficients are employed, which describe the response of the donor star's radius to mass loss. These coefficients are defined in Webbink (1985), as follows:

$$\zeta_{ad} \equiv \left(\frac{\partial \ln R}{\partial \ln M}\right)_{X,s} , \quad \zeta_L \equiv \left(\frac{d \ln R_L}{d \ln M}\right) , \quad \text{and} \quad \zeta_{eq} \equiv \left(\frac{\partial \ln R_{eq}}{\partial \ln M}\right)_X , \tag{2}$$

where ζ_{ad} is a logarithmic derivative of the donor's radius with respect to mass, at a constant chemical composition and specific entropy, ζ_L is the logarithmic derivative of the donor's Roche lobe radius with respect to its mass, and ζ_{eq} is the logarithmic derivative of the radius of the donor in thermal equilibrium, when held at a fixed chemical composition, with respect to mass. The mode of accretion is determined from the following inequalities between the coefficients

$\zeta_L < (\zeta_{ad}, \zeta_{eq})$ Nuclear time scale mass transfer. Mass transfer is not self-sustaining, and is strongly dependent on the degree to which the Roche lobe is overfilled. The resulting mass transfer rate is

$$-\dot{M}_2 = f(M_2) \ \ln\left(\frac{R_2}{R_L}\right)^3 \ \mathrm{M}_\odot \ \mathrm{yr}^{-1} , \tag{3}$$

where M_2, R_2, and R_L refer to the mass, radius and Roche lobe radius of the donor star, and $f(M_2)$ is given by

$$f(M_2) = 3 \times 10^{-6} \ [\min(M_2, 5.0)]^2 . \tag{4}$$

This relation is chosen to ensure steady mass transfer (Hurley et al. 2002, and references therein).

$\zeta_{eq} < \zeta_L < \zeta_{ad}$ Mass transfer occurs on the thermal time scale of the donor's envelope. If M is the donor mass, M_c is the core mass of the donor, and τ_{kh} is the Kelvin-Helmholtz time scale (in years) of the donor envelope, then the mass transfer rate is

$$-\dot{M}_2 = \frac{M_2 - M_c}{\tau_{kh}} \ \mathrm{M}_\odot \ \mathrm{yr}^{-1} . \tag{5}$$

$\zeta_{ad} < \zeta_L$ Dynamical mass transfer. In this situation, the radius of the primary expands more quickly than the Roche surface after transferring a mass element. Thus the mass-loss rate is limited only by the sound speed in the envelope of the donor, and is a runaway process.

If τ_{dyn} is the sound-crossing time of the donor (the donor's radius divided by the envelope sound speed), then the mass-loss rate is just

$$-\dot{M}_2 = \frac{M_2 - M_c}{\tau_{dyn}} \ \mathrm{M}_\odot \ \mathrm{yr}^{-1} \ . \tag{6}$$

A number of HMXBs exhibit a very different mode of mass transfer; namely, accretion from a strong stellar wind coming off of a massive companion, typically a Be- or O-star. We do not consider these systems for a number of reasons. First, the X-ray luminosity of such an XRB is highly variable, and strongly tied to the positions of the two stars relative to the line of sight, as the absorption column density is far from isotropic. Second, these systems tend to be very faint (of order 10^{36} erg s^{-1} or less; see, for example, Yokogawa 2002), unless in a rare outburst from an instability in the companion. While these sources have a hard X-ray spectrum, their luminosities are very low and they are never present in sufficient concentration to dramatically alter the outcome of the simulation.

Pulsars and the associated supernova remnants (SNRs) also contribute to the overall X-ray luminosity. While SNRs can attain luminosities of 10^{37}erg s^{-1} and above (Martin et al. 2002), much of this radiation is emitted below 2 keV, while we are interested in the hard X-ray emission in the 2–10 keV band. We also ignore isolated, rotation-powered pulsars and their associated synchrotron nebulae since their contribution is not significant unless the bulk of newly-formed pulsars would require spin periods of 10 ms or less (see the discussion of Van Bever & Vanbeveren 2000).

2.4. Mass Accretion, Stability, and Resulting X-ray Luminosity

For the Roche-lobe overflow systems we are considering here, the accretion flow, collimated through the inner Lagrange point, naturally forms into a disk structure around the accretor, as it cannot shed angular momentum quickly enough to permit a direct impact onto the primary (Shakura & Sunyaev 1973). A distinction must be drawn between the mass transfer rate (the rate of material passing through the inner Lagrange point), and the mass accretion rate (the rate of material accreting on to the compact object). Clearly, the X-ray luminosity is determined by the latter. In a conservative mass transfer scenario, no matter is lost from the system, and the two transfer rates should be equal if the disk remains in steady state. This is not generally true, however, and we must quantify the extent to which mass transfer is non-conservative. We can establish a relation defined in terms of the Eddington luminosity limit of the accretor; so the mass transfer rate $-\dot{M}_2$, and mass accretion rate $\dot{M}_1$, are related by

$$\dot{M}_1 = (\alpha_{Edd} - 1) \ \dot{M}_2 \ , \tag{7}$$

where

$$\alpha_{Edd} = \max \left(0 \ , \ 1 - \frac{\dot{M}_{Edd}}{|\dot{M}_2|} \right) \tag{8}$$

The $\dot{M}_{Edd}$ term is the mass accretion rate that generates a luminosity equal to the Eddington luminosity of the accretor. In other words, as the mass transfer rate climbs above $\dot{M}_{Edd}$, the mass transfer becomes increasingly non-conservative, as α_{Edd} approaches unity.

The prescription for converting a mass transfer rate into a bolometric luminosity follows from energy conservation. Assuming that the accreting matter falls effectively from infinity onto the surface of a compact object of radius r_1, the total available power is

$$L_{bol} = \frac{GM_1\dot{M}_1}{r_1} \ . \tag{9}$$

Half of the potential energy liberated by the infalling material is released in the accretion disk before making contact with the compact object (e.g., Pringle 1985). Precisely where this energy is emitted becomes important when considering accretion onto a black hole, where energy crossing the event horizon cannot be radiated. Thus, we introduce the efficiency parameter η_{bol}, with a value of 0.5 for black hole accretors, representing the fraction of energy released before the accreting material disappears across the event horizon. For neutron star accretion, we take this value to be unity, with essentially all of the energy radiated from either the inner accretion disk and boundary layer or from the accretion column, in the case of a strongly magnetized object.

A second efficiency factor, η_{st}, that must be considered is the duty cycle of the accreting systems. In particular, the dramatic high-luminosity, soft-spectrum and low-luminosity, hard-spectrum states observed in Galactic HMXBs such as Cygnus X-1 and GS 1124–68 can be understood as a transition between a bright, optically-thick disk and a dim, radiatively-inefficient accretion flow (Meyer et al. 2000). Such transitions are thought to be the result of an instability analogous to the "dwarf nova" instability seen in many cataclysmic variables. A thorough analysis of the physics that drives the instability can be found in Frank et al. (1992, p. 104) and Hameury et al. (1990). Since we cannot compute the structure and stability properties of the accretion disk, we adopt an empirical approach based on observational information. It is known that LMXB systems with black hole accretors (BH/LMXBs), for example, almost always exhibit the dwarf nova instability. For neutron-star LMXBs (NS/LMXBs) this is much less common. It is thought that significant X-ray emission from accretion on to the neutron star illuminates and heats the disk, maintaining the high-viscosity state and allowing stable accretion (van Paradijs 1996; King et al. 1996; King 2001).

For the purposes of our simulation, we have broken down this problem into three possible cases, as follows:

1. *Accretion onto a neutron star primary from a massive companion (high- or medium-mass X-ray binaries; a.k.a. NS/HMXB or NS/MMXB).* – This is the simplest case. The generally high mass transfer rates from massive companions, coupled with the radiation from the surface of the neutron star, act to prevent the dwarf nova instability. We therefore take the duty cycle of such systems to be unity.

2. *Accretion onto a neutron star from a low-mass companion (NS/LMXB).* – Here, the lower mass transfer rate means less illumination of the accretion disk by accretion onto the neutron star. To determine if the instability manifests itself in a given system of this type, we employ a period criterion inferred from figure 3 in Li & Wang (1998). The critical period P_{crit} is

$$\log P_{crit}\ (\mathrm{days}) = 6.5 \left(\frac{M_2 - 0.6}{\mathrm{M}_\odot} \right) \ , \tag{10}$$

where M_2 is the donor mass, as before. If the donor mass is below 0.6 $M_\odot$, the energy released by mass transfer is judged to be insufficient to stabilize the disk, regardless of the orbital separation of the system. If 0.6 $M_\odot < M_2 <$ 0.8 $M_\odot$, then the system is taken to be stable if the orbital period is less than the critical period P_{crit} above. If M_2 exceeds 0.8$M_\odot$, then the system is stable only if its period is less than twenty days. All systems with larger periods are assumed to exhibit the dwarf nova instability, and are assigned a duty cycle of 0.1, meaning that each system has a 10% chance of being counted in the overall X-ray luminosity. This value is on the high end of a typical duty cycle for soft X-ray transients (Tanaka & Shibazaki 1996).

3. *Black hole accretors from a companion of any mass.* – Because there is little radiation from the vicinity of the compact object illuminating the disk, a black hole system must be closely bound to avoid the disk instability. The criterion for this case is taken from King (2001), where it is derived from estimating when the luminosity required to suppress disk outbursts exceeds the Eddington luminosity. The critical period for the system in this case is

$$P_{crit} \simeq 3.3 \left(\frac{f_{disk}}{0.7}\right)^{-1.5} \left(\frac{\dot{M}_2}{0.5\ \dot{M}_{Edd}}\right)^{0.75} \left(\frac{M_1}{M_2}\right)^{0.125} \quad \text{days} \tag{11}$$

The f_{disk} term refers to the disk filling fraction, which is the ratio of the disk radius to the radius of the accretor's Roche lobe. We estimate this radius as the point at which the disk is disrupted by the tidal forces exerted by the donor star. Those systems with periods above P_{crit} are flagged as subject to the dwarf nova instability. The duty cycle of such systems is known to be dramatically shorter than for neutron star accretors with this disk instability. This is because, in the absence of illumination from accretion onto a stellar surface, more material must be added to the disk to raise the temperature to the point where steady accretion can occur, and this material takes more time to accumulate. Typical recurrence times are on the order of a decade or longer (Chen et al. 1997) ,implying duty cycles of 0.01 or lower. With such extended recurrence times, it is difficult to estimate a mean time between outbursts, as few transient systems have been observed in outburst more than twice. For now, we assume a duty cycle of 0.01, keeping in mind that this will likely change as more black hole transient systems are catalogued.

A final efficiency parameter, η_x, is employed to convert the calculated bolometric luminosity to the power radiated between 2–10 keV. This factor varies with the type and spin of the accreting compact object. For simplicity (and because the code does not track spin), we assume that 40% of the bolometric luminosity from accretion onto a black hole is emitted in this band. For neutron star accretion, that value is 20%. This adjustment is used everywhere that an X-ray luminosity is quoted herein.

To summarize, the integrated 2–10 kev luminosity of the populations is computed as

$$L_{2-10\ \mathrm{keV}} = \sum_{\text{all XRBs}} \eta_{st}\ \eta_x\ \eta_{bol}\ L_{bol}\ , \tag{12}$$

where the last term represents the total available accretion power as given by equation (9) and all the other terms are the efficiency factors discussed above. The first efficiency factor, η_{st}, which

represents the duty cycle of accretion-disk instabilities, is a true multiplicative factor only in the ideal case of an infinitely large population of XRBs. In practice, however, we are dealing with a finite number of systems and the effect of instabilities is a stochastic fluctuation of the X-ray luminosity, as individual systems experience high and low states. This behavior is particularly obvious at late times when only a small number of systems contribute to the observed X-ray luminosity. In order to capture this stochastic behavior, we have adopted a monte-carlo approach to assigning values to η_{st}. More specifically, for each system we assign a value of either 0 or 1 to η_{st} with a probability determined by the instability duty cycles noted above. This correction is also applied to the number of "active" systems presented with our results in the following section.

3. Simulation Results

Four simulation runs were performed, each simulating a 20 Myr episode of star formation, at a constant rate of 10 $M_\odot$ yr^{-1}. Of the four simulations, two were performed using the Salpeter initial mass function (Salpeter 1955), and two with the Miller-Scalo IMF (Miller & Scalo 1979). For each IMF, one run was performed with a flat mass ratio distribution, $\psi(q) = constant$, and the other draws the mass ratio from the distribution $\psi(q) = 2/(1+q)^2$, which approaches the spectroscopically-determined distribution shown in equation (1). For ease of reference these shall be referred to hereafter as "Sal/flat q", "Sal/low q", "MS/flat q", and "MS/low q".

The first question to address is the normalization of the simulations; that is, how one converts from a desired star formation rate and duration to a total number of binaries generated. Since the code draws the primary mass from an IMF that is truncated at 4 $M_\odot$ at the low end, we need a weighting factor, w, which is the number of generated stars of all masses divided by the number of generated stars above the 4 $M_\odot$ cutoff. In other words,

$$w = \frac{\int_{0.1}^{\infty} dN}{\int_{4}^{\infty} dN} \tag{13}$$

where dN is the differential number of stars with mass $m = M/M_\odot$, i. e., the IMF. Performing this integration we obtain $w = 145.5$ for the Salpeter IMF. Similarly, by considering the three separate power laws of the Miller-Scalo IMF, we obtain $w = 69.2$ for this case.

Next, a definition of the binarity fraction is needed. We take the binarity fraction b to represent the fraction of *systems* that contain two stars. For example, if a sample of three stars exists as a binary pair and one single star, the binarity is taken to be one-half (as opposed to two-thirds).

If we let $\bar{m}$ and $\bar{q}$ represent the average primary mass (in $M_\odot$) and binary mass ratio, respectively, and let n denote the total number of binaries formed per unit time (in a 1 Myr period), then the total SFR for the 1 Myr interval is the sum of three parts; the mass contributed by the primary stars, the mass contributed by the companion stars (weighted by $\bar{q}$), and the mass of the single stars which are not considered in the code but are generated according to the binarity b. Assuming a binarity of $b = 0.5$, we can then write

$$\mathrm{SFR} = nw\bar{m} + nw\bar{m}\bar{q} + nw\bar{m}\left(\frac{1-b}{b}\right) = nw\bar{m}(2+\bar{q}) \tag{14}$$

We note that $\bar{m}$ and $\bar{q}$ are functions of the IMF and mass ratio distribution, respectively, while w is a function of the IMF. The values of each of these parameters for the four runs are shown in Table 1. The last column of the table shows the number of binary systems generated for each Myr of the simulation, representing a constant 10 $M_\odot$ yr^{-1}SFR. The SFR varies linearly with the number of binaries formed in each interval, allowing the results to be adjusted for an arbitrary SFR by simple proportionality. This proportionality breaks down at large times, however, when large scatter is introduced by small-number statistics, as only one or two sources are active at any given moment.

One of the principal results of the simulations are the curves showing the time evolution of the 2–10 keV X-ray luminosity (calculated according to §2.4) and population size of the X-ray luminous population (with stochastic corrections for high/low states applied). The population is subdivided into six categories, based on two intrinsic properties of the system. First, the accretor is classified as either a black hole or a neutron star. Second, the donor is placed in one of three mass categories. Donors with a mass less than 1.4 $M_\odot$ are LMXBs, donors with a mass between 1.4 and 8 $M_\odot$ (the minimum mass necessary to form a neutron star) are considered to be medium-mass X-ray binaries (MMXBs), and more massive donors are, naturally, HMXBs. Plots showing the evolution of the luminosity and size of each population subset are shown, one set for each of the four possible parameter sets. Figures 1–13 detail the final output of the investigation.

Figure 1 gives the most important and directly observable result; namely, the total 2–10 keV X-ray luminosity for the population, evolved over the first 2 Gyr after the star formation episode. The luminosity includes all efficiency factors, following equation (12). Panels (a) and (b) show the results for a Salpeter IMF, with a low-skewed and flat q-distribution, respectively, while panels (c) and (d) show the analogous plots for a Miller-Scalo IMF. It is apparent from Figure 1 that the input IMF and mass ratio distribution have little or no effect on the X-ray luminosity evolution of the population. This is an interesting and important result, because it implies that the output depends little upon uncertainties in the IMF, or choice of q-distribution, both parameters with significant uncertainties. Conversely, however, this also means that it would be difficult to constrain these parameters through a comparison of the results with observational data.

Figure 2 shows the evolution of XRBs with black hole accretors, given an initial Salpeter IMF, and a low q distribution after equation (1). Each point represents the luminosity or population size for a 1 Myr interval. Star formation progresses at a constant rate for 20 Myr; the end of star formation is shown as a vertical dashed line on each of the plots. The left two panels (a and c) show the luminosity evolution of the HMXB and MMXB populations, respectively. No active BH/LMXBs were found in the first 2 Gyr epoch. The corresponding plots on the right side show the number of *luminous* X-ray emitting systems of each type at the indicated epoch (i. e., systems in their low states are excluded). The evolution of all systems was tracked out to a maximum of 2 Gyr, though massive systems evolve on more rapid time scales, and are only tracked until the second compact object is formed. Panel (a) shows the luminosity evolution for the BH/HMXB systems, with a peak at about 2×10^{40} erg s^{-1}, coinciding with the end of the star formation episode. This is understood to be the result of massive donor stars, with short main sequence lifetimes. HMXBs thus form very quickly after the creation of the initial binary, as the secondary (donor) star leaves the main sequence. The HMXB population tracks star formation closely, with accreting systems accumulating until star formation stops, at which point the remaining systems quickly die off; 20

Myr after the end of the star formation episode, no HMXBs remain. One final point: comparing the peak luminosity in panel (a) with the peak BH/HMXB population size in panel (b) of the same figure, we see that the mean luminosity of a binary is around 10^{38} erg s^{-1}. This corresponds to the Eddington luminosity limit for an accretor of roughly 5 $M_\odot$ (with all efficiency factors taken into account), which the typical black hole mass given the assumed IMF and the progenitor-to-black-hole mass mapping, discussed above. Thus, we conclude that the black holes, which dominated the hard X-ray luminosity at early times, accrete very close to their Eddington limit.

Continuing with Figure 2, panels (c) and (d) detail the evolution of BH/MMXB population, with companion masses ranging from 1.4–8 $M_\odot$. The first and most important thing to notice is the delay in the onset of this population. The first such systems do not appear until more than 10 Myr have elapsed, and their numbers do not peak until about 30 Myr after the end of star formation. This is a result of the longer evolutionary time scales of these less-massive companion stars. The black hole forms quickly, but the binary will only enter the accretion stage on the nuclear time scale of the donor star. This concentration of sources and corresponding peak in X-ray luminosity at $\sim$ 50–60 Myr is a result of two effects. First, because of the choice of mass ratio distribution, a primary massive enough to form a neutron star (at least 8 $M_\odot$) is less likely to have a light companion. For a flat mass ratio distribution, the average companion mass for an 8 $M_\odot$ star is 4 $M_\odot$. For the low-skewed mass ratio distribution, this value drops to just under 3 $M_\odot$. This is a selection effect of sorts, arising from the minimum mass necessary to form a neutron star. The second factor to consider is that the duration of a typical mass transfer episode occupies a larger fraction of the life of a massive star than a star at the light end of the MMXB category ($\sim$ 1.4 $M_\odot$). Since massive companions are formed on a time scale comparable to their main sequence lifetimes, they all tend to leave the main sequence and fill their Roche lobes in a similarly short period. This contributes to the luminosity peak in panel (c). Longer-lived stars are less likely to leave the main sequence in closely-timed groups, spreading out the resulting X-ray binaries in time. These sources are not concentrated in time, but XRBs from this group continue to "turn on" even at very large times (several Gyr).

One other feature of note in panel (c) is the bifurcation in the luminosity evolution that occurs about 70 Myr into the simulation. This population oscillates rapidly between a low-luminosity and a high-luminosity state. A glance at the number evolution plot shows that, at this epoch, less than ten sources (and at times as few as two) comprise the entire MMXB group. The variation is therefore partly due to small number statistics, as single sources flicker in and out of mass transfer episodes. As well, in the systems comprising the upper branch of the bifurcation the companion star is crossing the Hertzprung Gap, implying a rapid expansion and commensurately high mass transfer rate and luminosity. The lower systems tend to be transferring matter on the nuclear time scale of the companion, with a lower resulting luminosity per system.

Figure 3 is analogous to Figure 2, and shows the evolution of populations in which the compact object is a neutron star rather than a black hole. All run parameters remain identical. Panels (a) and (b) are almost precisely the same as those of the previous figure, with the exception of a noticeable delay in the rise-time of the NS/HMXB population. This is directly related to the longer main sequence lifetime of the lighter neutron star progenitors.

Panels (c) and (d) show the evolution of the NS/MMXB set. This is the most numerous

population, and, at its peak value is the most luminous as well, for a brief period from roughly 40–80 Myr into the simulation. The evolution curves are quite smooth, until around 200 Myr, when the XRB population size fluctuates rapidly between several and ten or twenty sources at a time, with a corresponding dramatic fluctuation in the luminosity. The slow decrease in the maximum luminosity as the population ages results from fewer accreting systems, and also lower mass transfer rates from increasingly lighter, longer-lived companion stars. It is interesting to note, however, that the luminosity of this subset of XRBs remains significant well beyond even 2 Gyr. This means that populations of NS/MMXBs formed in long-vanished starbursts continue to contribute to the X-ray luminosity of their host galaxy, long after the galaxy return to quiescent star formation. This also means that successive waves of rapid star formation may allow NS/MMXBs and NS/LMXBs to accumulate, so that the total number of such systems observed in the present era represents a number of individual starbursts taking place in the distant past.

Panels (e) and (f) show the NS/LMXBs. Note that they also attain a significant luminosity, at a later epoch than the MMXB population. One might expect that no such systems would be present in the first 2 Gyr of the simulation, as the main sequence lifetime of even the most massive companions in this category (1.4 $M_\odot$) is significantly longer than that. These systems are all survivors of an episode of common envelope evolution, during which the primary star ascended the giant branch, and enveloped the secondary. The small orbital separation required for the companion to fill its Roche-lobe is unlikely to have occurred *ab initio* given the distribution of initial orbital separations. The dramatic reduction in orbital separation during this phase meant that, after the primary went through a supernova, the secondary was close enough to begin transferring mass onto the nascent neutron star. The small probability of this outcome explains the relatively small number of systems in this category.

The relationship between the high-mass and lower-mass XRB systems, could best be summarized as follows. The BH/HMXB and NS/HMXB populations track the *current*, or *recent* star formation rate. MMXBs and LMXBs, however, better track the *time-integrated star formation* in a galaxy's history, i. e., the total mass of stars formed.

A quantity that is easily observable and can also be computed from the results of our simulations is the luminosity function. If one assumes that the luminosity function is a power law of the form

$$N(L) \equiv N_0 \, L^{-\gamma} \quad (\text{with } \gamma > 0), \tag{15}$$

the *cumulative* luminosity function is

$$N(> L) \equiv \int_L^\infty N(L) \, dL = N_1 \, L^{-\beta} \quad (\text{for } \gamma \neq 1), \tag{16}$$

where $\beta = \gamma - 1$ and $N_1 = N_0/(1-\gamma)$. The cumulative luminosity function is the quantity most often derived from observations. With this in mind, we show in Figures 10–13 the cumulative luminosity function at five epochs (10 Myr, 20 Myr, 50 Myr, 100 Myr and 200 Myr) after the beginning of star formation. The luminosity function is expressed in terms of the fractional amount of the population that exists above a given luminosity. One interesting aspect of these functions is that, because they represent a time-slice of the luminosity evolution, longer-lived systems are more likely to be included. This makes them representative, but the high-luminosity sources, which are only active

for a short time, may be missed. This means that the high end of all of the displayed luminosity functions is subject to a considerable amount of variability as short-lived, high-luminosity systems flicker on and off. To circumvent this, we consider at each epoch 100 time slices, separated by 10^4 years. For each of these slices, we calculate a luminosity function, and then plot the extremes of these functions as solid and dashed lines.

Table 2 shows the measured power-law indices of the cumulative luminosity functions of Figure 10 and those immediately following. The ranges given correspond to the extremes of the luminosity function at each epoch, as discussed in the previous paragraph. As can be seen from this table, the principal determining factor for this quantity is the elapsed time since the end of star formation. This is because the luminosity function becomes dramatically steeper as the population ages and luminous X-ray sources die off. In principle, one could use this value to estimate the age of a stellar population. In practice, this would require a great deal of detailed information about the star formation history of the host galaxy, in order to segregate individual stars by the particular star-formation episode which spawned them. We will return to the cumulative luminosity function and other observables in §6, to compare our predictions with the results of recent observations.

4. Discussion of Simulation Results

An important question is the overall robustness of the results with respect to several other variables that are not explicitly listed as input variables, but comprise assumptions made in the implementation of the population synthesis code. We now describe each of these in detail, along with probable effects on the output, and a justification for the choice of parameter value employed.

As mentioned previously, our choice for mass loss through winds during the main sequence phase is taken from the work of Langer (1989). This is the canonical treatment of winds used in the majority of the literature. A more recent formulation by Hamann & Koesterke (1998) dramatically lowers the wind-loss rate on the main sequence, and is used in the numerical simulations of Van Bever & Vanbeveren (2000). This has the consequence of keeping the binary separation smaller throughout the main sequence evolution (as a larger mass loss would widen the system dramatically). As well, stars retain a larger fraction of mass prior to the supernova, resulting in larger compact object masses. The end result is closer, more massive systems that are more likely to survive the first supernova without becoming unbound. This results in a greater number of potential XRBs, and a correspondingly larger X-ray luminosity. As an example, the results of Van Bever & Vanbeveren (2000) show an X-ray luminosity several times greater than in our own simulations, resulting from a factor of four decrease in wind mass loss. The wind prescription of Hamann & Koesterke (1998) has only been applied to a few systems. Until confirmed by further observations, the formulation of Langer (1989) is still a very reasonable choice for describing winds.

Magnetic breaking of the secondary star was taken into account via the model of Eggleton (2001), which relates the torque to the properties of the star, assuming that the secondary is in synchronous rotation with the orbit of the binary. Although the adopted prescription is relatively simple, magnetic breaking is an important effect only in the case of stars with convective envelopes, i.e., the secondaries of LMXBs. Since LMXBs make only a small contribution to the integrated X-ray luminosity, the precise prescription for magnetic breaking has a minimal effect on our results.

The mapping between the mass of a black hole progenitor and the final mass of the hole (the black hole "IMF") is another poorly-constrained quantity. We make use of the IMF derived by Fryer (1999), using hydrodynamic collapse models. Critical to the end result is the mass at which a progenitor will collapse directly to a black hole, with no intervening supernova (and hence no asymmetric kick, discussed below). This limit strongly influences the average resulting black hole mass, as objects above the limit tend to retain most or all of their pre-collapse mass, and objects below this limit lose a substantial fraction of this mass through a supernova. If the critical collapse limit is high, most black holes will experience a supernova at formation, with a lower resulting mass. If this limit set low, the average black hole mass will be much greater, with correspondingly narrower orbits and larger Eddington accretion rates. The results in Fryer (1999) do approximate the typical observed mass in black hole candidates (averaging around $\sim$ 6–7 $M_{\odot}$; Bailyn et al. 1998). However, this observable is likely influenced by selection effects dependent on the mass of the black hole.

The effect of kick magnitude on the survival of a binary is discussed in Sipior & Sigurdsson (2002). The kick distribution chosen for our simulations is a single Gaussian consistent with the bimodal distribution of of Podsiadlowski et al. (2002), where a mix of low ($\sim$ 90 km s^{-1}) and strong ($\sim$ 450 km s^{-1}) kicks is shown to reproduce the distribution of observed neutron star velocities.

The Eddington limit is a somewhat contentious restriction on the maximum accretion rate of a compact object. In our models, we assume that the Eddington rate applies weakly; that is, the mass accretion rate is throttled back dramatically above this limit, with no abrupt cutoff. Still, this only permits a minor violation (typically of a few tens of percent) of the Eddington limit. However, there is observational evidence of systems that exceed this boundary by factors of several. For example, three X-ray pulsars in the Magellanic Clouds the are known to exhibit substantially super-Eddington luminosities (namely LMC X-4, SMC X-1, and A 0538–66; Nagase 1989; Woo et al. 1995, and references therein). Nevertheless, most galactic XRBs are at or below this limit, so this is representative of most known sources.

Lastly, we consider the parameter governing the efficiency of common-envelope evolution. Webbink (1984) introduced the idea of of simulating a phase of common-envelope evolution by decreasing the orbital energy by the binding energy of the envelope. The efficiency parameter was assumed to be unity, so that the two quantities were equal. Later work by de Kool (1990) showed that when compared against reasonable stellar models, the average efficiency parameter dropped to around 0.5, and this is the value we use. This value means that the orbit must lose twice the binding energy of the envelope in order to dissipate it. It is true, however, that the precise value of the efficiency parameter depends strongly on the structure of the evolving star. More recently, Dewi & Tauris (2000) showed that the efficiency value ranged between 0.2 and 0.8 for the vast majority of stellar evolution tracks. Unfortunately, the code we are using does not track the structure of the star closely enough for us to be able to incorporate this more accurate prescription. Nevertheless, it is clear that the mean parameter value is a good choice overall for calculating the end results of a common-envelope evolution phase. Increasing the parameter would result in wider systems, and hence fewer XRBs. However, the fact that fewer systems would merge under these conditions would mitigate this somewhat. A lower value of the efficiency parameter would dramatically increase the number of mergers, with fewer systems surviving this phase to become XRBs.

5. Comparison With Other Theoretical Work

Recently, a number of attempts have been made by various groups to use population synthesis techniques to estimate the X-ray luminosity of a star formation episode at various epochs. We discuss three of them here, and draw a comparison between the results and methodology.

5.1. Numerical Simulations by Van Bever & Vanbeveren

The simulations of Van Bever & Vanbeveren (2000) are nearest to our own work in terms of technique. A sizable population of binary systems was generated, using a library of stellar evolution calculations detailed in Vanbeveren et al. (1998a,b,c). Winds, in particular, receive a great deal of attention, as the precise mass loss formalism used can greatly affect the final evolutionary outcome of massive stars. In particular, the choice of wind strength will change the mass distribution of black holes seen in the population, as the black hole progenitor loses a different amount of mass prior to collapse. As mentioned above, our simulations make use of the wind mass loss formalism of Langer (1989). Van Bever & Vanbeveren (2000) make use of the mass loss rates of Hamann & Koesterke (1998), which are roughly four times smaller than those predicted by Langer, and include the effects of line blanketing and clumping in determining wind strengths. The result of these stronger winds are wider binaries, but with a larger fraction surviving the initial supernova. More black hole mass measurements are needed to lend support to the low wind mass loss rates; in particular, a large population of black holes with confirmed masses above ~ 10 $M_\odot$ would require winds considerably weaker than those predicted by Langer (1989).

Another significant difference in the assumptions made by Van Bever & Vanbeveren (2000) involves the final collapse of a massive star to a black hole. They assume that all such objects (those with an initial mass of above 25 $M_\odot$) collapse directly to a black hole, with no associated supernova event. This again has the effect of increasing the mean black hole mass, as no material can be lost from the system via a supernova. They themselves note that there is observational evidence contravening this assumption; specifically, the dramatic overabundance of O, S, Mg and Si in the atmosphere of the optical component of the LMXB GRO J1655–40, reported by Israelian et al. (1999). The primary in this system is a strong black hole candidate, with an inferred mass of $6 \pm 2 M_\odot$. Our own simulations assume that a star with a zero age main sequence (ZAMS) mass of 20 $M_\odot$ or more will become a black hole. Those progenitors with a ZAMS mass of less than 40 $M_\odot$ are assumed to undergo a supernova upon black hole formation. Above this limit, the hole forms via direct collapse, with no explosion. The difference is important, because black holes that form through direct collapse should experience no natal kicks, which can act to disrupt the system. The result is that a greater fraction of systems with a black hole survive to become X-ray binaries. For the same reason, a greater fraction of the observed XRB population will comprise accreting black holes, since neutron stars will still experience kicks at the same rate as before.

Van Bever & Vanbeveren (2000) generate a single burst of 3×10^5 stars, selecting the masses of single stars and binary primaries from a Salpeter IMF. A flat q distribution is used to choose the mass for the companion star. Single stars are tracked in this model because the hard (2–10 keV) X-ray contribution from supernova remnants (SNRs) is included in the total. To do this, neutron stars

are assigned a magnetic field strength and initial spin period chosen from a random distribution, which allows the rotational energy loss rate to be calculated. A small fraction (~ 0.03) is then used to determine the amount of this energy that emerges as X-rays. We do not include young supernova remnants in our own calculations, for two reasons. First, the assignment of a magnetic field and rotational period at formation ignores the importance of the evolutionary history of the progenitor star, and so is fairly arbitrary. Second, the contribution of remnants to the total X-ray luminosity should be quite small for all but the shortest period pulsars. Indeed, after completing their simulation, Van Bever & Vanbeveren (2000) come to very much the same conclusion, claiming that SNRs contribute to the total starburst X-ray luminosity only when most or all neutron stars are born with an initial period of less than 10 ms.

Van Bever & Vanbeveren (2000) plot the X-ray luminosity evolution for the first 10 Myr after the starburst. The onset time for the X-ray luminous phase is 3–4 Myr, precisely the same as in our own simulations. The peak *specific* luminosity of around 10^{33}erg s^{-1} M$_\odot^{-1}$ is reached shortly thereafter (around 5 Myr), and remains constant through the 10 Myr that are plotted. This is very different from our own results, which show that the X-ray luminosity continues to rise nearly 100 Myr after the end of star formation, though the rate of increase slows dramatically after star formation ends. By only tracking the population out to 10 Myr, Van Bever & Vanbeveren (2000) missed the important contribution of neutron star accretors to the overall X-ray luminosity over an extended period of time. Note that the specific luminosity is given in terms of a power per unit solar mass of stars generated. If we scale the luminosity results shown in Figure 1 by dividing the peak luminosity by the total mass of stars formed in each simulation (2×10^8 M$_\odot$), we obtain a specific luminosity of approximately 5×10^{32} erg s^{-1} M$_\odot^{-1}$, almost exactly the peak rate given by Van Bever & Vanbeveren (2000).

One last thing to note about both the results of Van Bever & Vanbeveren (2000) and our own simulations is the strongly stochastic behavior of the luminosity evolution. This is noticeable throughout the 10 Myr range considered by the former, and can be seen in our results at longer time scales (typically above 100 Myr). This is the direct result of small-number statistics, when few systems are in an active state at a given time. The Van Bever & Vanbeveren (2000) results are based on a relatively small initial population of 3×10^5 stars, many of which will not become XRBs. Our larger population size of 2×10^6, and the fact that the star formation occurs over a significant interval, helps to smooth out dramatic fluctuations in the luminosity until a much larger period of time has elapsed.

5.2. Analytic Calculation by Wu

As an alternative to the population modeling shown heretofore, where individual systems are tracked from birth to evolutionary end state, Wu (2001) views a population of XRBs in terms of differential equations governing birth and death rates. Unfortunately, to formulate such a system of equations requires a slew of simplifying assumptions. In particular, Wu assumes perfectly circular initial orbits to calculate gravitational radiation and magnetic braking time scales, and completely ignores the effects of natal kicks from supernovae. In addition, no allowance is made for disk instability effects. As well, the parameterization of many input quantities make comparison

with observables difficult, with no clear coupling to a SFR. To keep the system integrable analytically, the initial population and birth rate of binaries are taken as somewhat ad hoc power-laws in luminosity. Also, the lifetime for X-ray luminosity is taken to be inversely proportional to the binaries luminosity, implicitly assuming that all donors supply an identical amount of mass. Still, the method has the advantage of rapidly exploring a wide parameter space, as well as providing analytic relations between certain parameters that would not be immediately obvious from numerical population synthesis.

A comparison of the results from Wu (2001) is complicated by the fact that no easy way exists to adjust his results to a SFR. Wu presents a number of luminosity functions representing the distribution of XRBs at a given epoch, but no normalization is possible. Nevertheless, it is interesting to note that the bulk of the cumulative luminosity functions shown by Wu (2001) display a distinct turnover at a luminosity of around 6×10^{37} erg s^{-1}, a turnover which is also clearly visible in many of the luminosity functions resulting from our own simulations, and roughly one-third of the Eddington luminosity of a typical neutron star. As more work making use of this technique appears, a better comparison of these two dramatically different approaches to population synthesis may be possible.

5.3. Semi-Analytical Calculation by Ghosh & White

Ghosh & White (2001) make use of a related methodology through which they use X-ray survey data to infer the long-term evolution of cosmic SFRs. They also establish a system of differential equations describing the population of X-ray binaries, though their approach is more rooted in experimental data, and is couched in terms of a real SFR, as opposed to the parameterized version found in Wu (2001).

The goal of this study is quite different from our own, and is focused on the X-ray luminosity evolution over time scales of a Hubble time. Our work is in rough agreement in a qualitative sense; that is, the relative contribution of the various XRB species is similar, and the shape of the luminosity curves are analogous. We differ in one major prediction, however. Ghosh & White predict that the LMXB population will not become a significant contributor to the total X-ray luminosity until several Gyr have passed; in other words, when the companion stars either begin evolving off the main sequence, or lose sufficient orbital energy to magnetic braking and/or gravitational radiation. Our prediction is that a large number of LMXB systems will become active in the first 200 Myr or so after a vigorous star formation episode; e. g., panels (e) and (f) on any of Figures 2–9. These systems are survivors of a stage of common-envelope evolution, which shrank the orbital radius and permitted Roche-lobe overflow to occur several billion years before it would otherwise be possible. Ghosh & White do not consider the effect of common-envelope evolution in their equation set, and so do not predict this feature.

6. Comparison With Observations

We close by comparing some of our major predictions with observations. The computed quantities that are readily comparable to observations are the integrated X-ray luminosity of the population and the general shape of the luminosity function and its evolution. Further and more detailed tests must take the form of case studies, where the X-ray properties of well-studied star-forming systems are compared with customized simulations that make use of the specific properties of those systems (such as the SFR, the age of the starburst, and the star-formation history).

Recently, Ranalli et al. (2003) extended the well-known correlation between a galaxy's far-infrared (and radio) luminosities and the underlying SFR to the 2–10 keV energy regime (an earlier form of this correlation was also presented by Helfand & Moran 2001). Making use of and *ASCA* *BeppoSAX* observations of nearby actively-star forming galaxies, they proposed that the SFR could be related to the 2–10 keV luminosity of the host galaxy by

$$\mathrm{SFR} = 2.0 \left(\frac{L_{2-10\ \mathrm{keV}}}{10^{40}\ \mathrm{erg\ s^{-1}}} \right)\ \mathrm{M_\odot\ yr^{-1}}\ . \tag{17}$$

For our simulated galaxy experiencing an SFR of 10 $\mathrm{M_\odot\ yr^{-1}}$, we found that the peak hard X-ray luminosity, reached at the time star formation ceases and sustained for several tens of Myr, was around 4×10^{40} erg $\mathrm{s^{-1}}$. As discussed earlier, this result is largely independent of the choice of IMF or binarity fraction. By the above relation, such a galaxy should have an underlying SFR of 8 $\mathrm{M_\odot\ yr^{-1}}$, which is in good agreement with the actual rate used in the simulation. This reinforces our original claim that the principal output of our simulations is robust.

Grimm et al. (2003) show a number of cumulative luminosity functions based upon recent *Chandra* and ASCA observations of nearby starbursts. The cumulative luminosity functions of twelve noted starbursts were fitted to a relation describing the fall off of the luminosity function at the high end. They derive a best-fit power-law index of $\beta = 0.6$, which can be compared to our results in Table 2. Grimm et al. (2003) do not discuss the variation in this index with time (as the stellar population evolves), thus we compare their results to our cumulative luminosity function slopes at early times as most of the objects in their study are still actively star-forming. While still slightly steeper than those of Grimm et al. (2003), our index at 10 Myr, especially for the Miller-Scalo IMF, is in agreement with the observations. It should also be noted that the power-law indices measured for the individual galaxies have a substantial spread to them and are in general agreement with our predicted range of values. Similar measurements for smaller sets of galaxies (Eracleous et al. 2002; Kilgard et al. 2002), are in closer agreement with our steeper cumulative luminosity function. Our cumulative luminosity functions show the correct behavior, as they become both steeper and fainter with increasing time. This point is at the heart of the observed difference between the luminosity functions of spiral galaxies and ellipticals (Zezas et al. 2002). As well, elliptical galaxies are generally more massive than the systems generated by our simulations, so that the chance of finding rare, exceptionally luminous sources (i. e., with black hole primaries descended from the very high end of the IMF) increases dramatically. Such sources would affect the slope of the luminosity function, but they are unlikely to be predicted by our simulations.

This work was supported by NASA through grant GO0-1152A,B from the Smithsonian Astrophysical Observatory. MSS acknowledges additional support from the Zaccheus Daniel Foundation. SS acknowledges support from NSF grant PHY-0203046 and from the Center for Gravitational Wave Physics, which is supported by the NSF under cooperative agreement PHY 01-14375. We thank Vicky Kalogera Krzys Belczynski for very useful discussions.

REFERENCES

Abt, H. A. 1983, ARA&A, 21, 343

Arzoumanian, Z., Chernoff, D. F., & Cordes, J. M. 2002, ApJ, 568, 289

Bailyn, C. D., Jain, R. K., Coppi, P., Orosz, J. A. 1998, ApJ, 499, 367

Batten, A. H., Fletcher, J. M., & MacCarthy, D. G. 1989, Catalogue of the orbital elements of spectroscopic binary systems: 8: 1989 (Victoria: Dominion Astrophysical Observatory)

Begelman, M. C. 2002, ApJ, 568, L97

Blaauw, A. 1961, Bull. Astron. Inst. Netherlands, 15, 265

Bloom, J. S., Sigurdsson, S., & Pols, O. R. 1999, MNRAS, 305, 763

Caldwell, N., Kennicutt, R., Phillips, A. C., & Schommer, R. A. 1991, ApJ, 370, 526

Chen, W., Shrader, C. R. & Livio, M. 1997, ApJ, 491, 312

Condon, J. J. 1992, ARA&A, 30, 575

de Kool, M. 1990, ApJ, 358, 189

Devereux, N. A. & Young, J. S. 1990, ApJ, 350, L25

Dewi, J. D. M., & Tauris, T. M. 2000, A&A, 360, 1043

Duquennoy, A., & Mayor, M. 1991, A&A, 248, 485

Eggleton, P. P. 2001, in Evolution of Binary and Multiple Star Systems, ASP Conf. Ser. 229, eds. P. Podsiadlowski, S. Rappaport, A. R. King, D. D'Antona, & L. Burderi (San Francisco: ASP), 157

Elson, R. A. W., Sigurdsson, S., Davies, M., Hurley, J., & Gilmore, G. 1998, MNRAS, 300, 857

Eracleous, M., Shields, J. C., Chartas, G., & Moran, E. C. 2002, ApJ, 565, 108

Fabbiano, G., Zezas, A., & Murray, S. S. 2001, ApJ, 554, 1035

Frank, J., King, A., & Raine, D. 1992, Accretion Power in Astrophysics (Cambridge: Cambridge University Press)

Fryer, C. L. 1999, ApJ, 522, 413

Fryer, C. L., & Heger, A. 2000, ApJ, 541, 1033

Fryer, C. L., Heger, A., Langer, N., & Wellstein, S. 2002, ApJ, 578, 335

Ghosh, P., & White, N. E. 2001, ApJ, 559, L97

Gourgoulhon, E., & Haensel, P. 1993, A&A, 271, 187

Griffiths, R. E., Ptak, A., Feigelson, E. D., Garmire, G., Townsley, L., Brandt, W. N., Sambruna, R., & Bregman, J. N. 2000, Science, 290, 1325

Grimm, H.-J., Gilfanov, M., & Sunyaev, R. 2002, MNRAS, 339, 793

Habets, G. M. H. J. 1986, A&A, 167, 61

Hamann, W.-R., & Koesterke, L. 1998, A&A, 335, 1003

Hameury, J.-M., King, A. R. & Lasota, J.-P. 1990, ApJ, 353, 585

Hansen, B. M. S., & Phinney, E. S. 1997, MNRAS, 291, 569

Heckman, T. M. 1980, A&A, 87, 152

Heggie, D. C. 1975, MNRAS, 173, 729

Helfand, D. J. & Moran, E. C. 2001, ApJ, 554, 27

Hogeveen, S. J. 1992, Ap&SS, 196, 299

Hurley, J. R., Tout, C. A., & Pols, O. R. 2002, MNRAS, 329, 897

Irwin, J. A., Sarazin, C. L., & Bregman, J. N. 2002, ApJ, 570, 152

Israelian, G., Rebolo, R., Basri, G., Casares, J., & Martín, E. L. 1999, Nature, 401, 142

Janka, H.-T., & Mueller, E. 1994, A&A, 290, 496

Janka, H.-T., & Mueller, E. 1996, A&A, 306, 167

Kennicutt, R. C. 1983, ApJ, 272, 54

Kennicutt, R. C. 1998, ARA&A, 36, 189

Kilgard, R. E., Kaaret, P., Krauss, M. I., Prestwich, A. H., Raley, M. T., & Zezas, A. 2002, ApJ, 573, 138

King, A. R. 2001, in Black Holes in Binaries and Galactic Nuclei, eds. L. Kaper, E. P. J. van den Heuvel, & P. A. Woundt (ESO Workshop), 155

King, A. R., Davies, M. B., Ward, M. J., Fabbiano, G., & Elvis, M. 2001, ApJ, 552, L109

King, A. R., Kolb, U., Burderi, L. 1996, ApJ, 464, L127

Kuiper, G. P. 1935, PASP, 47, 121

Langer, N. 1989, A&A, 220, 135

Li, X.-D., & Wang, Z.-R. 1998, ApJ, 500, 935

Lira, P., Ward, M., Zezas, A., Alonso-Herrero, A., & Ueno, S. 2002, MNRAS, 330, 259

Livio, M. & Soker, N. 1988, ApJ, 329, 764

Lonsdale Persson, C. J., & Helou, G. 1987, ApJ, 314, 513

Maeder, A., & Meynet, G. 1989, A&A, 210, 155

Martin, C. L., Kobulnicky, H. A. & Heckman, T. M. 2002, ApJ, 574, 663

Meyer, F., Liu, B. F., & Meyer-Hofmeister, E. 2000, A&A, 354, L67

Meyer, F., & Meyer-Hofmeister, E. 1983, A&A, 121, 29

Miller, G. E., & Scalo, J. M. 1979, ApJS, 41, 513

Nagase, F. 1989, PASJ, 41, 1

Paczynski, B. 1971, Acta Astronomica, 21, 417

Pfahl, E., Rappaport, S., Podsiadlowski, P., & Spruit, H. 2002, ApJ, 574, 364

Podsiadlowski, P., Nomoto, K., Maeda, K., Nakamura, T., Mazzali, P., & Schmidt, B. 2002, ApJ, 567, 491

Pols, O. R., & Marinus, M. 1994, A&A, 288, 475

Pringle, J. E. 1985, in Interacting Binary Stars ed. J. E. Pringle & R. A. Wade (Cambridge: Cambridge University Press), 1

Ptak, A., Griffiths, R., White, N., & Ghosh, P. 2001, ApJ, 559, L91

Ranalli, P., Comastri, A., & Setti, G. 2003, å, 399, 39

Rasio, F. A. & Livio, M. 1996, ApJ, 471, 366

Ritter, H. 1988, A&A, 202, 93

Rosa-González, D., Terlevich, E., & Terlevich, R. 2002, MNRAS, 332, 283

Salpeter, E. E. 1955, ApJ, 121, 161

Shakura, N. I., & Sunyaev, R. A. 1973, A&A, 24, 337

Tanaka, Y. & Shibazaki, N. 1996, ARA&A, 34, 607–644

Telesco, C. M., Dressel, L. L., & Wolstencroft, R. D. 1993, ApJ, 414, 120

Van Bever, J., & Vanbeveren, D. 2000, A&A, 358, 462

Vanbeveren, D., de Donder, E., van Bever, J., van Rensbergen, W., & de Loore, C. 1998a, New Astronomy, 3, 443

Vanbeveren, D., de Loore, C., & van Rensbergen, W. 1998b, A&A Rev., 9, 63

Vanbeveren, D., van Rensbergen, W., & de Loore, C. 1998c, The brightest binaries (Dortrecht: Kluwer), 106

van Paradijs, J. 1996, ApJ, 464, L139

Webbink, R. F. 1984, ApJ, 277, 355

Webbink, R. F. 1985, in Interacting Binary Stars, eds. J. E. Pringle & R. A. Wade (Cambridge: Cambridge University Press), 39

White, N. E., & Ghosh, P. 1998, ApJ, 504, L31

Woo, J. W., Clark, G. W., & Levine, A. 1995, ApJ, 449, 880

Wu, K. 2001, Publications of the Astronomical Society of Australia, 18, 443

Yokogawa, J., 2002, Ph. D. Thesis, Kyoto University

Zezas, A., Fabbiano, G., Rots, A. H., & Murray, S. S. 2002, ApJ, 577, 726

Table 1. Normalization Parameters for Starburst Simulations

Simulation Parameters	$\bar{m}$ $(= \bar{M}/\mathrm{M}_\odot)$	$\bar{q}$	w	n (Myr^{-1})
Sal/flat q	0.39	0.500	145.5	71300
Sal/low q	0.39	0.386	145.5	74700
M-S/flat q	0.60	0.500	69.2	96300
M-S/low q	0.60	0.386	69.2	101000

Note. — Columns: (1) simulation identifier, which shows both the mass function and mass ratio distribution used, (2) mean mass of a star with the given IMF, (3) mean mass ratio of a companion to the primary, (4) conversion factor giving the total number of stars formed for every star formed above 4 $\mathrm{M}_\odot$, (5) the number of binary systems generated in each 1 Myr interval to give an SFR of 10 $\mathrm{M}_\odot$ yr^{-1}.

Table 2. Power-Law Index of Model Cumulative Luminosity Function at Five Epochs

Model	10 Myr	20 Myr	50 Myr	100 Myr	200 Myr
M-S / flat q	0.8–1.3	1.1–1.7	0.7–1.3	3.3–4.4	2.0–3.6
M-S / low q	0.8–1.1	1.1–1.5	1.1–1.8	2.9–5.7	2.9–5.7
Sal / flat q	1.2–2.5	1.3–1.9	1.4–3.6	2.9–5.7	2.9–5.0
Sal / low q	0.9–1.5	1.1–1.5	0.9–1.6	2.9–4.4	2.2–3.6

Note. — The measured ranges of the slope of a series of model luminosity functions. The model column refers to the assumed IMF and whether the mass ratio distribution is flat, or skewed towards low-mass companions.

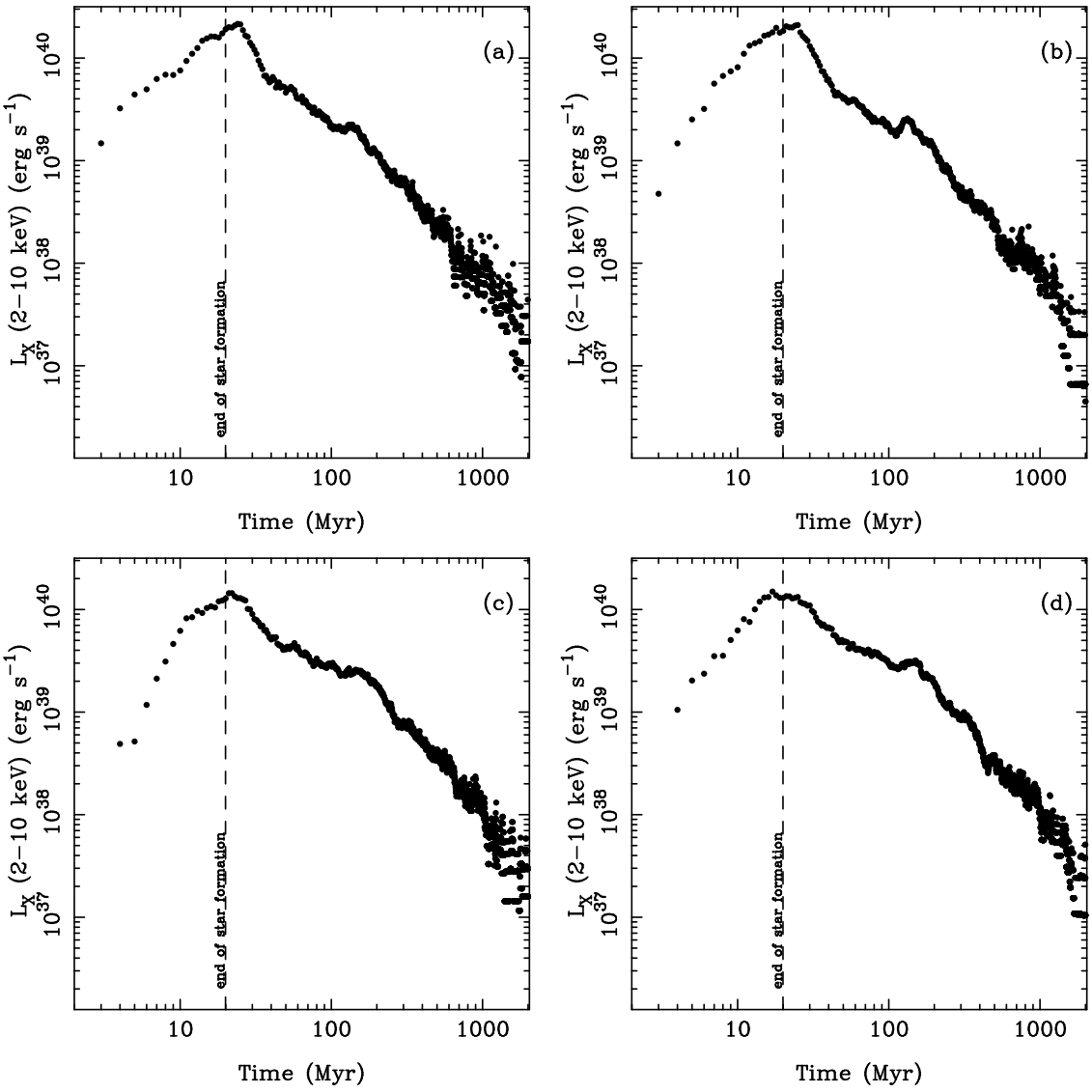

Fig. 1.— The evolution of the total 2–10 keV X-ray luminosity of a simulated population over 2 Gyr, from a SFR of 10 $M_\odot$ yr^{-1}, extending for 20 Myr (vertical dashed line). The luminosity includes all efficiency factors, following equation (12). Panel (a) shows the results of a Salpeter IMF with a low-skewed q-distribution. Panel (b) also uses the Salpeter IMF, with a flat mass ratio distribution. Panels (c) and (d) use the Miller-Scalo IMF with a low-skewed and flat mass ratio distribution, respectively.

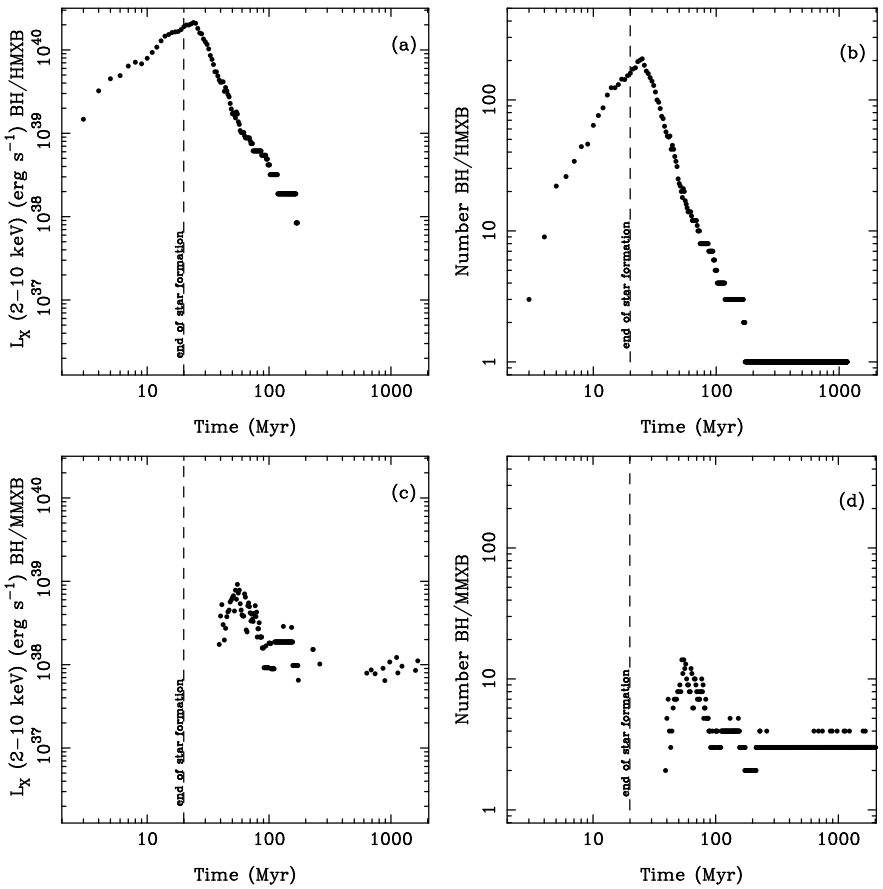

Fig. 2.— The evolution of the 2–10 keV luminosity of the BH/XRB component of the population over 2 Gyr, from a SFR of 10 $M_\odot$ yr^{-1}, extending for 20 Myr (vertical dashed line), for a Salpeter IMF and a low-skewed q-distribution. The luminosity plots include all efficiency factors, following equation (12). The population size plots show the number of *active systems* only (i. e., systems in a low state are excluded). Note the short delay between the start of the simulation and maximum luminosity, roughly corresponding to the nuclear lifetime of the secondary (donor) star. The luminosity evolution for (a) the BH/HMXB, and (c) the BH/MMXB populations are shown, alongside the evolution track of each population's size (b,d). No BH/LMXB population was detected in the first 2 Gyr epoch.

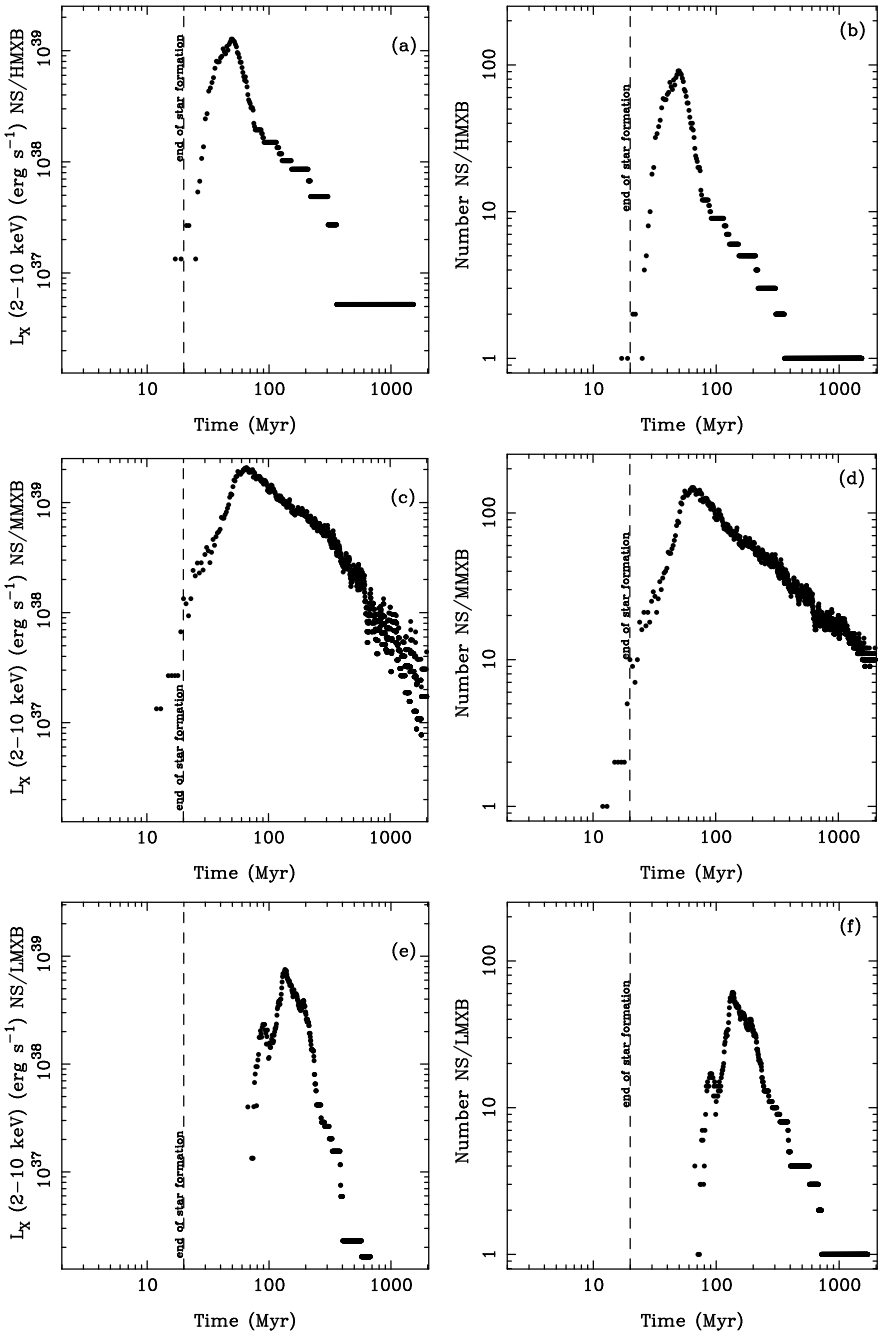

Fig. 3.— The evolution of the 2–10 keV luminosity and size of NS/XRB component of the population over 2 Gyr, from a SFR of 10 $M_\odot$ yr^{-1}, extending for 20 Myr, and for a Salpeter IMF with a low-skewed q-distribution. The luminosity plots include all efficiency factors, following equation (12). The population size plots show the number of *active systems* only (i. e., systems in a low state are excluded). This is the analogue of Figure 2 but for binaries with neutron star primaries. The luminosity evolution for (a) the NS/HMXB, (c) the NS/MMXB, and (e) the BH/LMXB populations are shown, alongside the evolution track of each population's size (b,d,f).

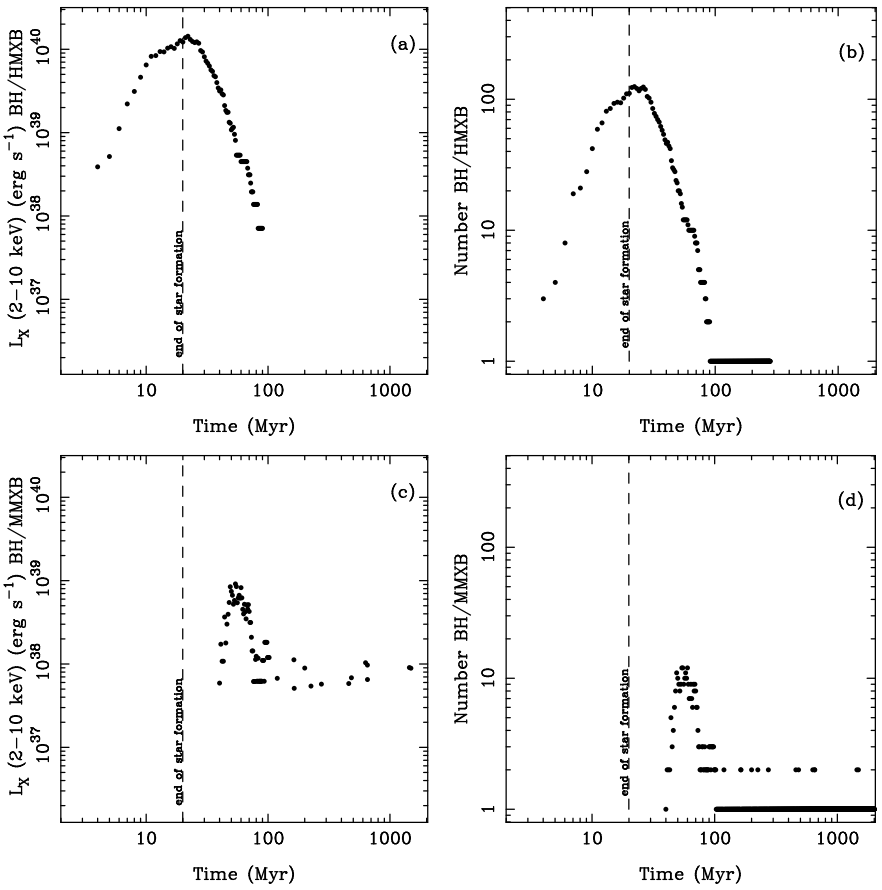

Fig. 4.— Same as Figure 2, for a Miller-Scalo IMF and a low q distribution.

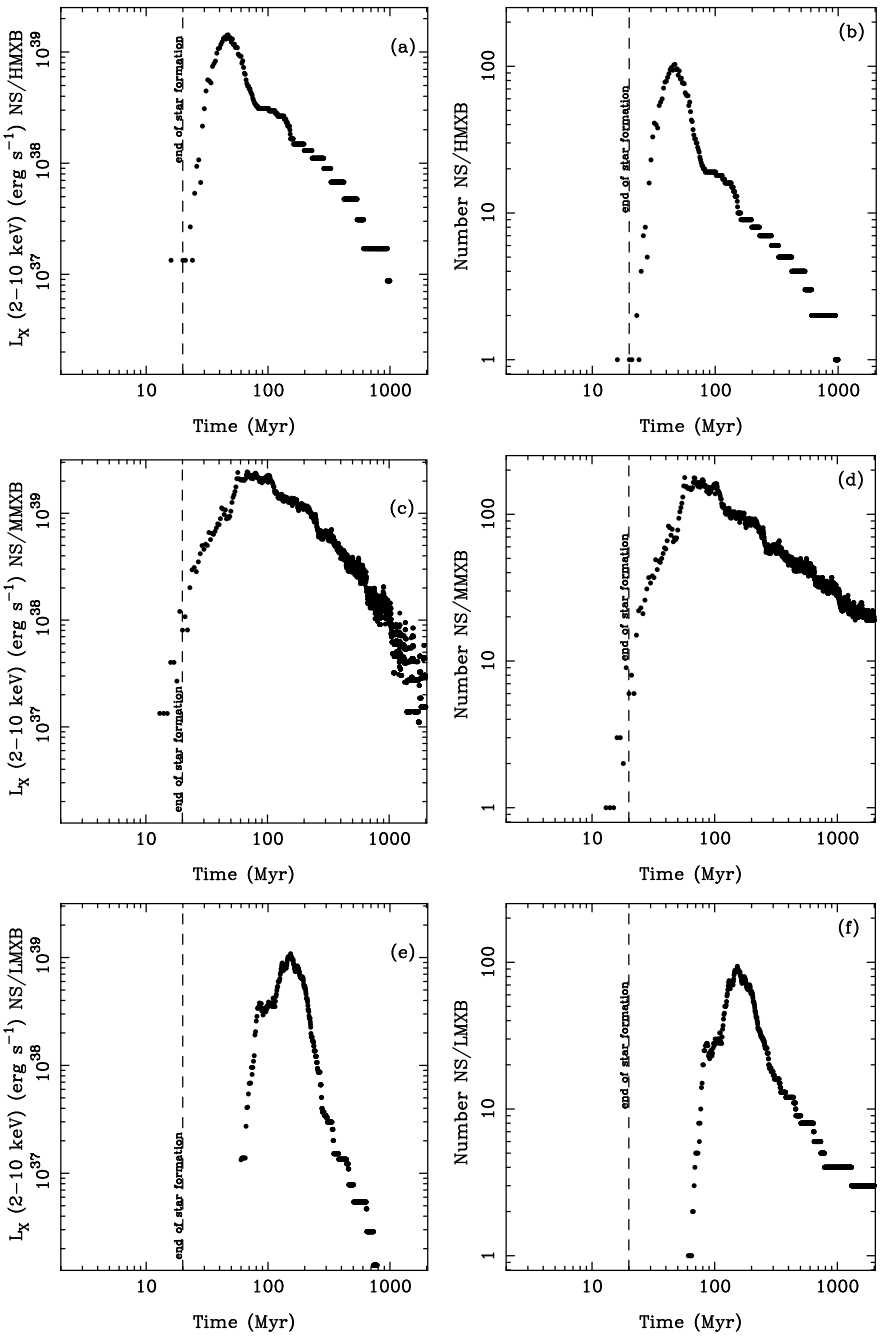

Fig. 5.— Same as Figure 3, for a Miller-Scalo IMF and a low q distribution.

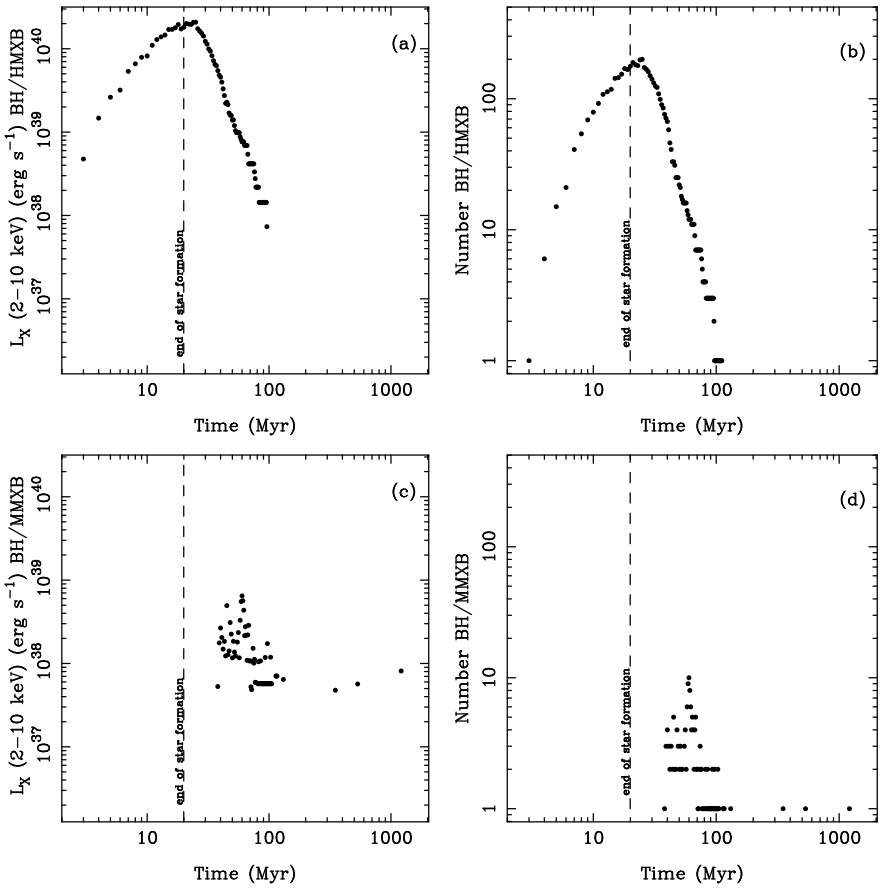

Fig. 6.— Same as Figure 2, for a Salpeter IMF and a flat q distribution (all values of q equally likely).

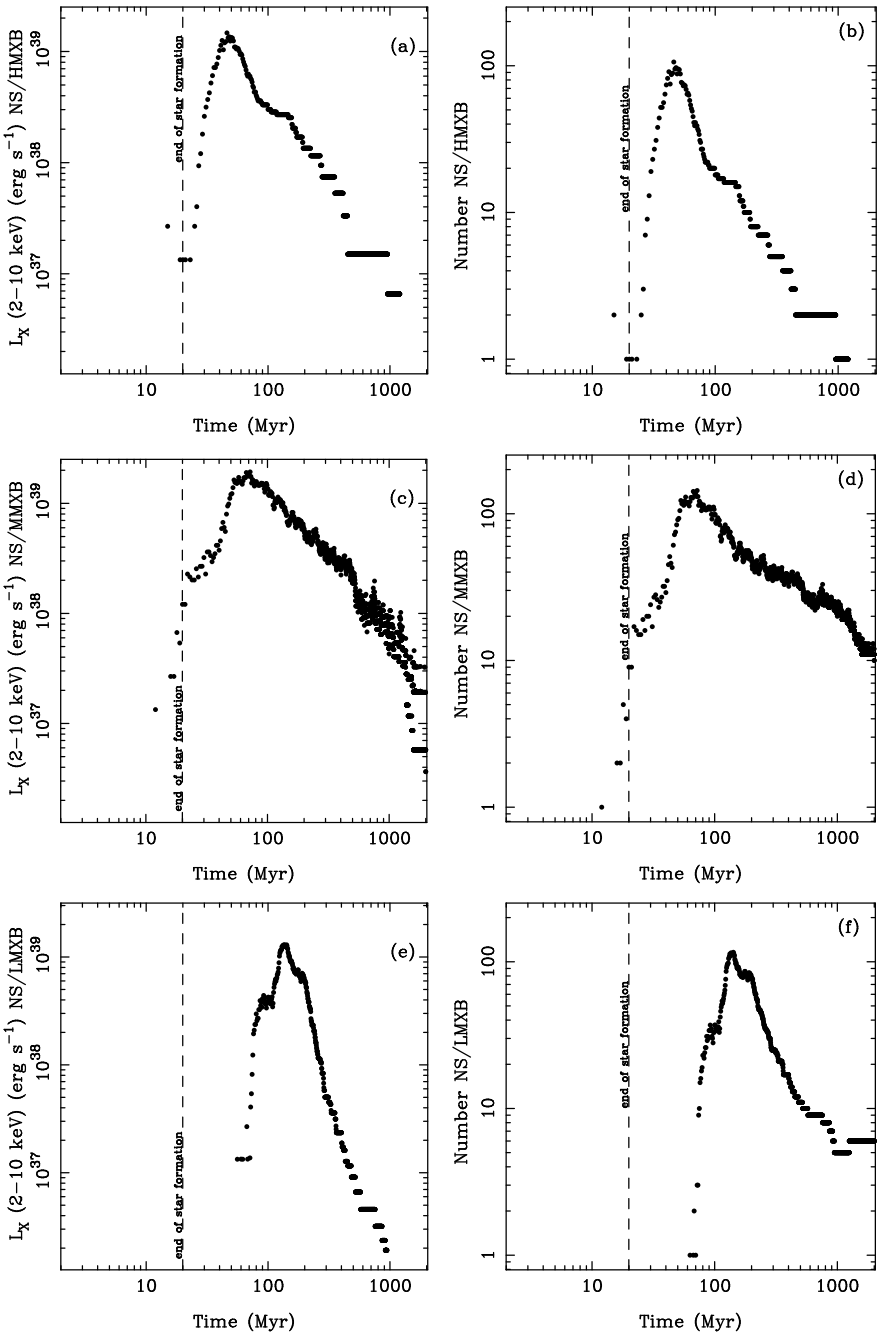

Fig. 7.— Same as Figure 3, for a Salpeter IMF and a flat q distribution (all values of q equally likely).

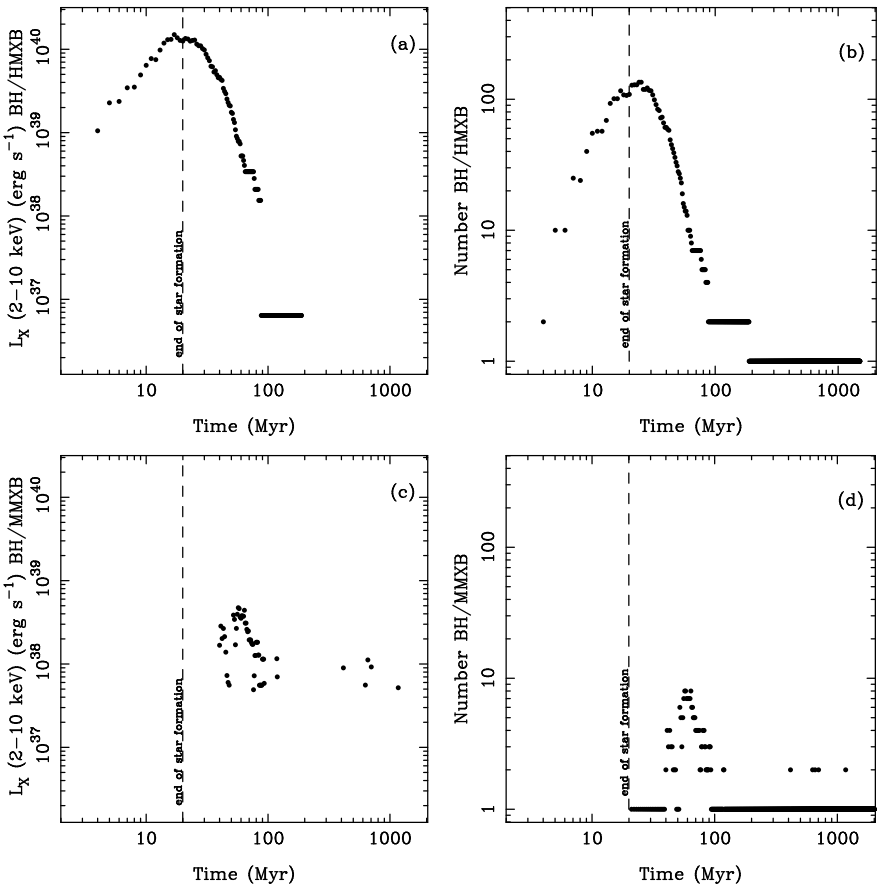

Fig. 8.— Same as Figure 2, for a Miller-Scalo IMF and a flat q distribution.

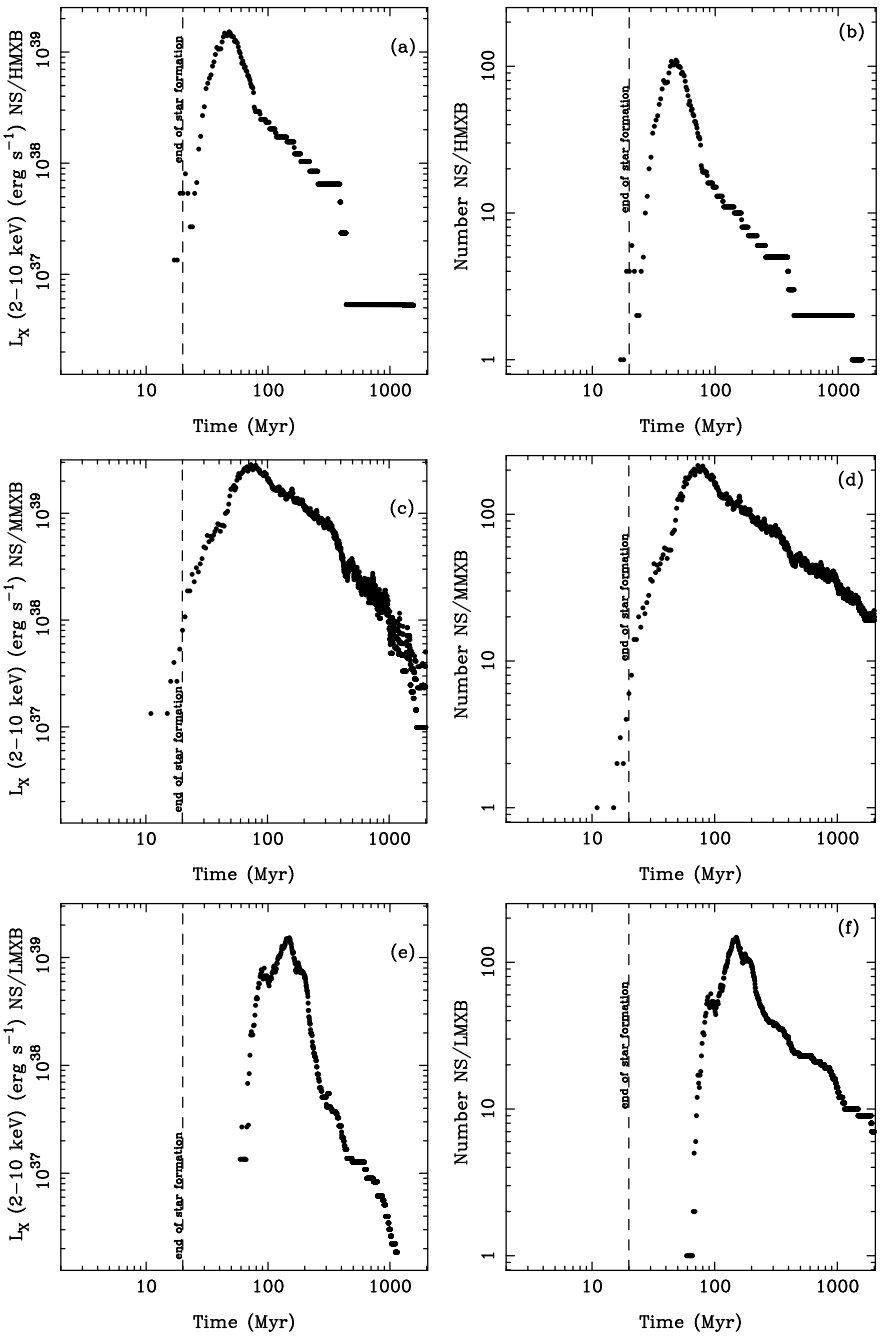

Fig. 9.— Same as Figure 3, for a Miller-Scalo IMF and a flat q distribution.

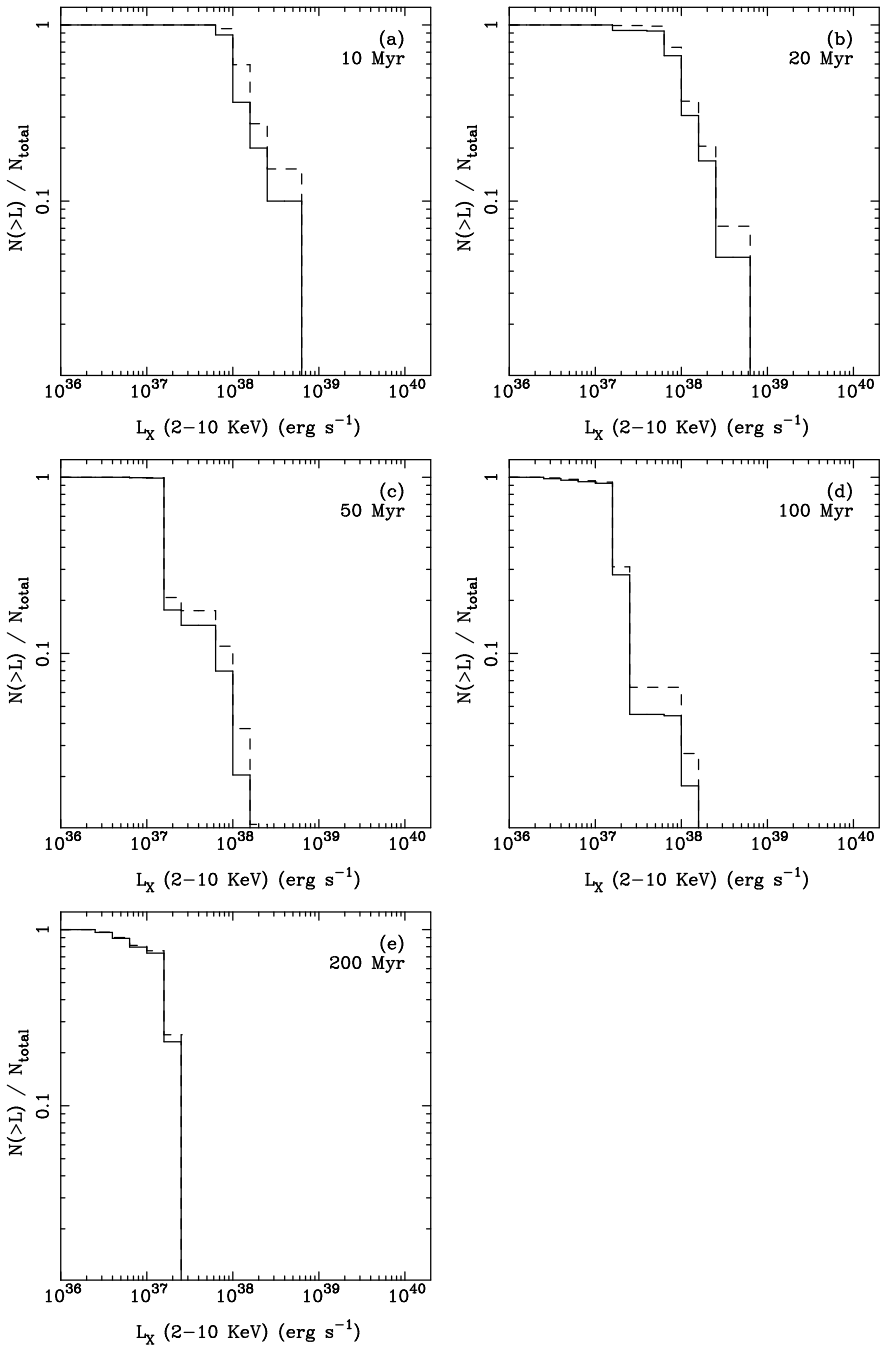

Fig. 10.— The cumulative luminosity function for the population derived from the Salpeter IMF, and a low-skewed q distribution. The five epochs are (a) 10 Myr, (b) 20 Myr, (c) 50 Myr, (d) 100 Myr, and (e), 200 Myr. These were chosen to show the dramatic change as star formation ends and massive stars no longer dominate (a and b), as the X-ray luminosity becomes driven by systems with increasingly lighter secondaries (c, d and e). The solid an dashed lines show the upper and lower bounds of this function, resulting from shirt-term stochastic variations in the number of active systems (see §2.4 and §3 for details).

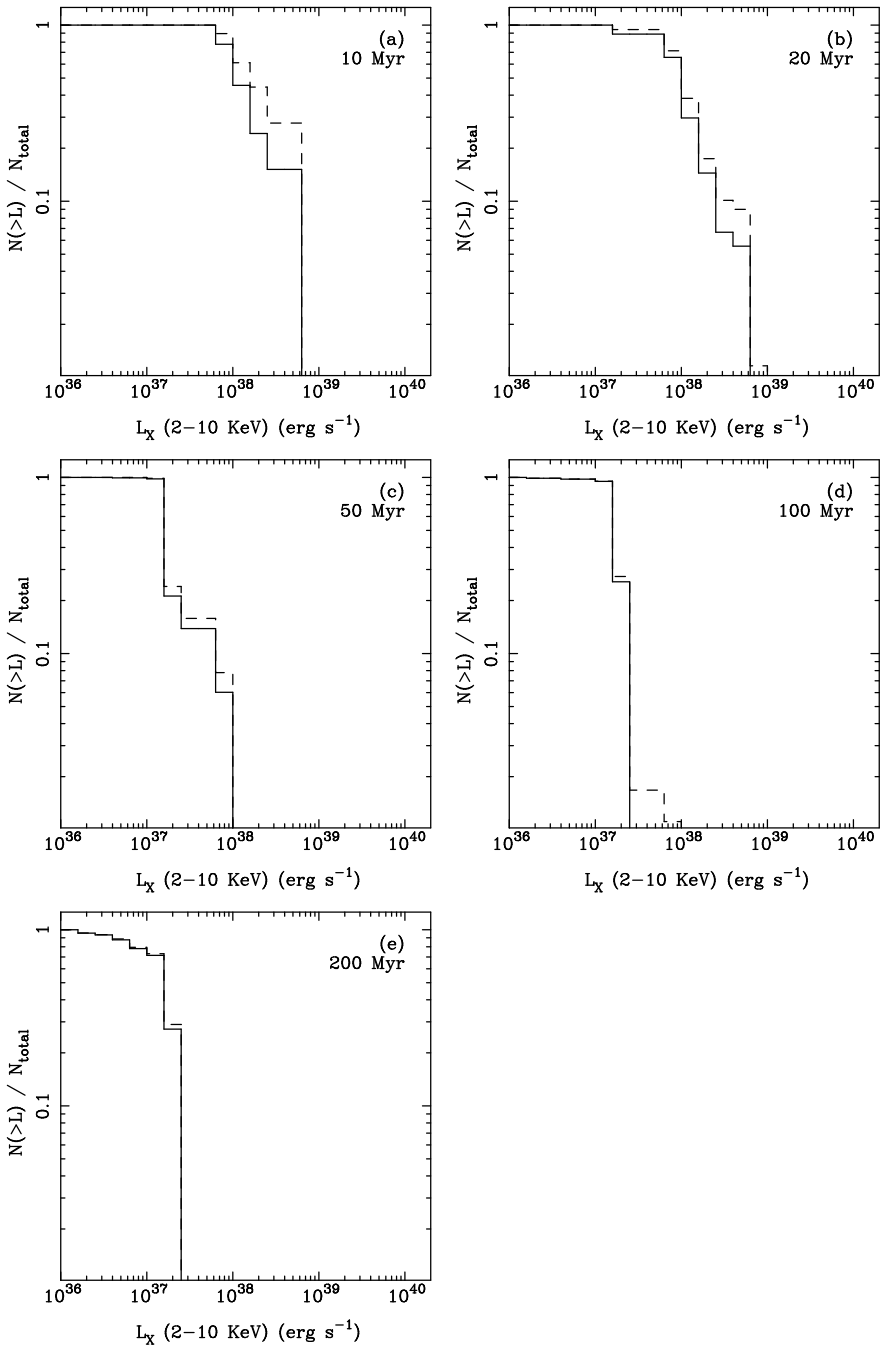

Fig. 11.— Same as for Figure 10, for a Miller-Scalo IMF and a low q distribution.

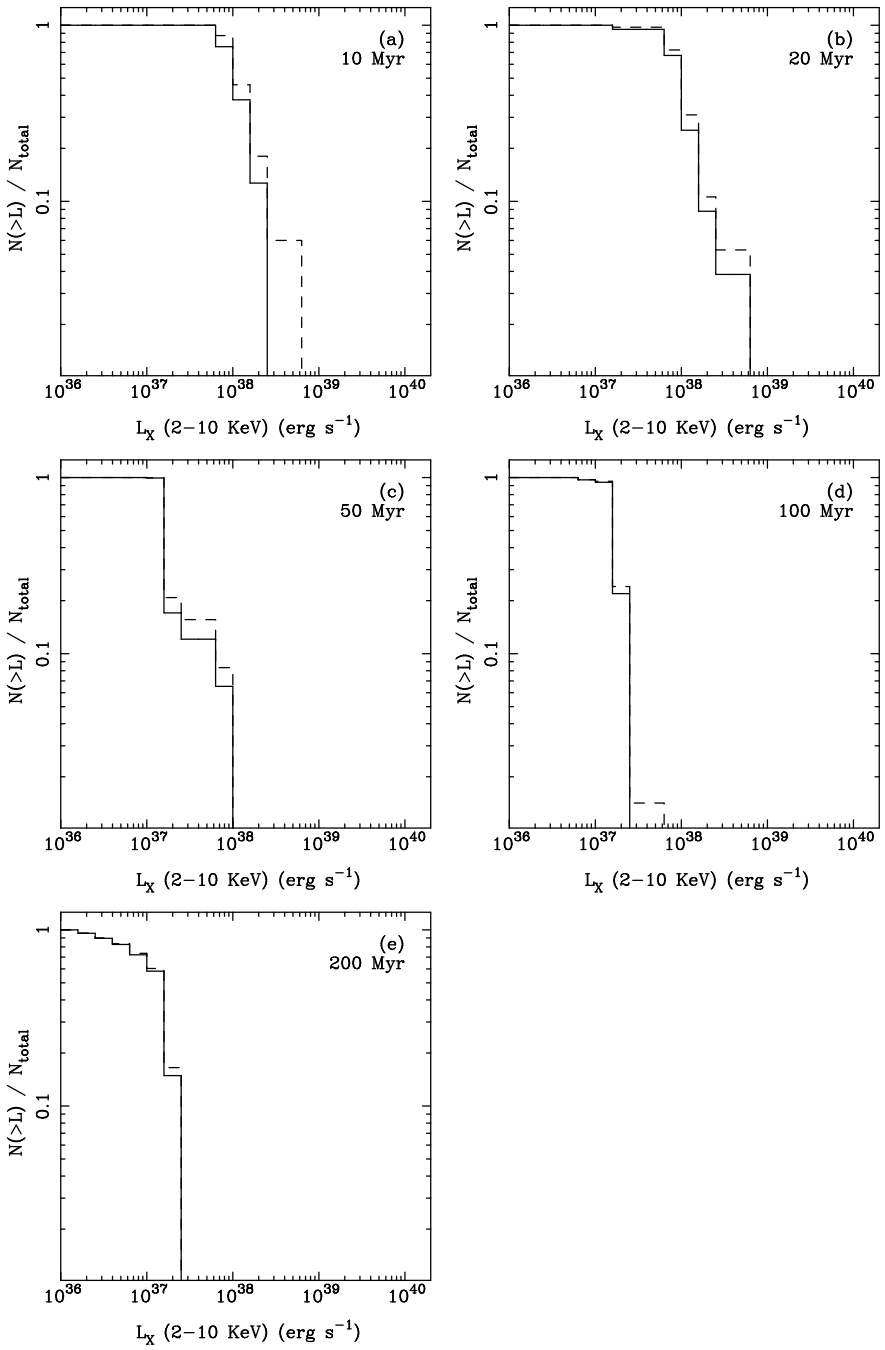

Fig. 12.— Same as for Figure 10, with a Salpeter IMF and a flat q distribution.

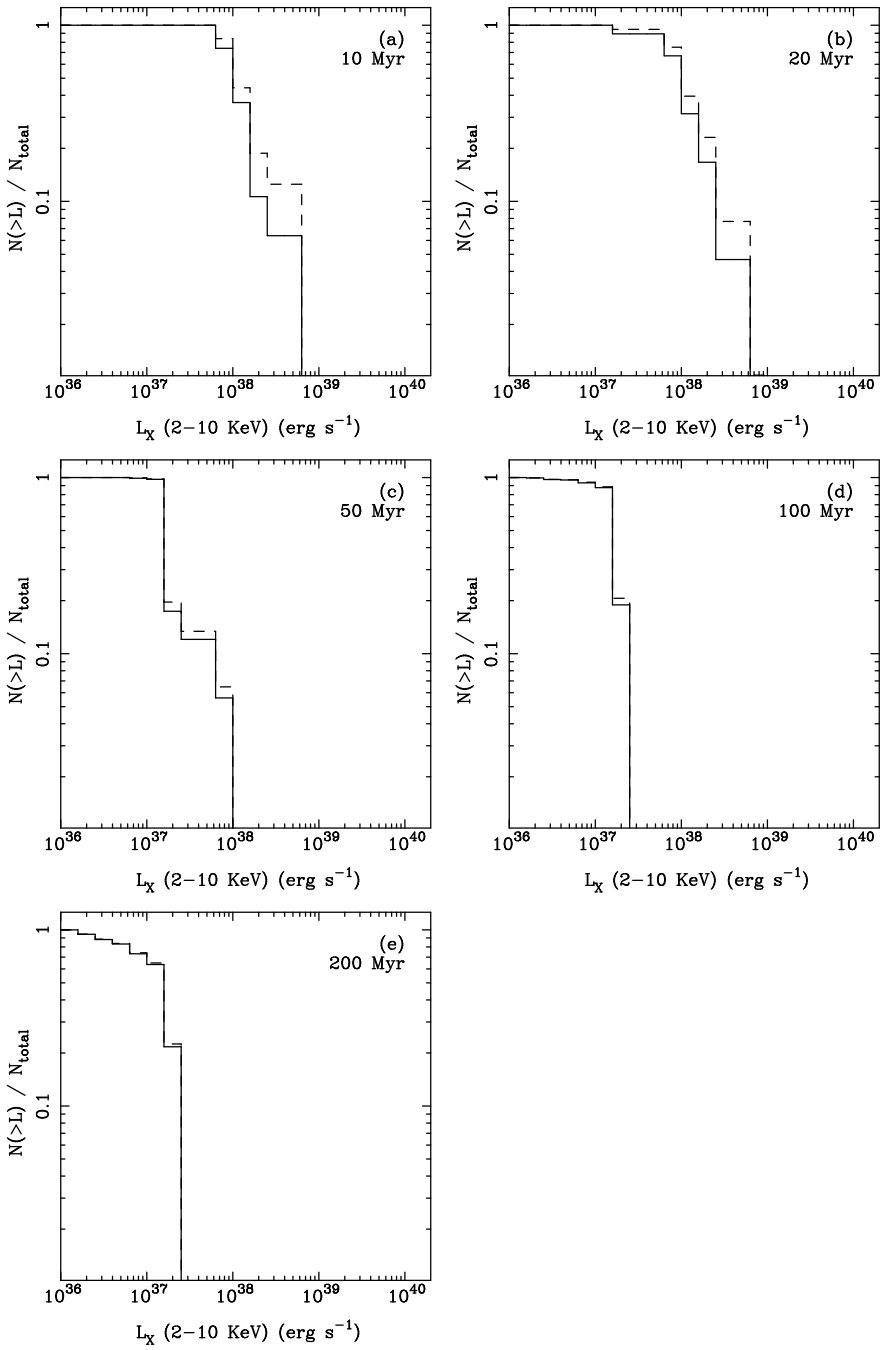

Fig. 13.— Same as for Figure 10, with Miller-Scalo IMF, and a flat q distribution.